iScience

Article

Auditory evoked delta brushes involve stimulus-specific cortical networks in preterm infants

Graphical abstract

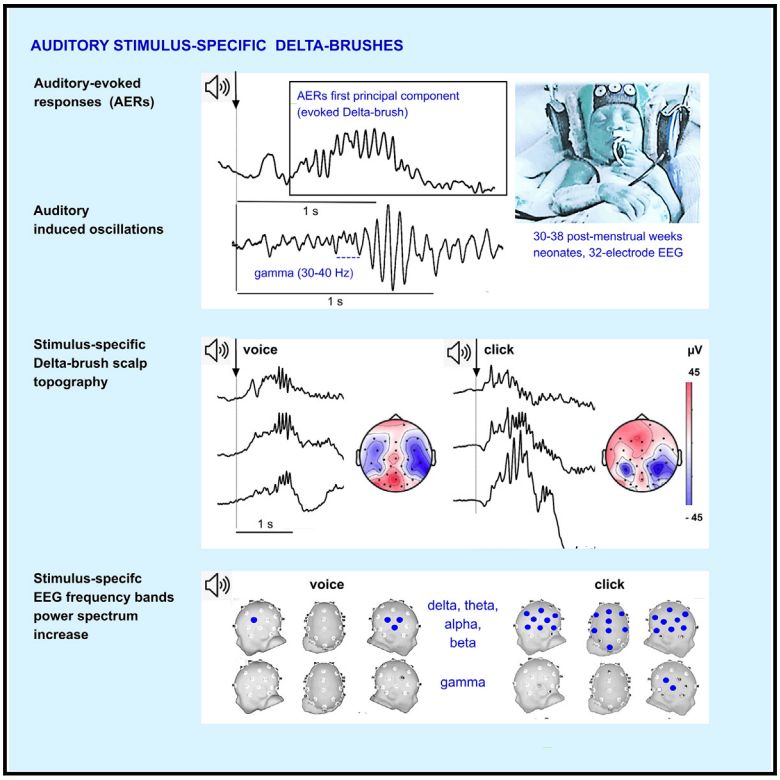

Highlights

- In preterm babies, auditory evoked Delta-brushes (DBs) include gamma oscillations
- Evoked DBs scalp topography depends on the physical characteristics of the auditory stimulus
- Evoked oscillations are more widespread after the click compared to vocal stimulus
- Evoked DBs prevail on the right but shift to the left with age after the vocal stimulus

Authors

Anna Kaminska, Dorothée Arzounian, Victor Delattre, ..., Mathieu Kuchenbuch, Jessica Dubois, Roustem Khazipov

Correspondence

anna.kaminska@aphp.fr

In brief

Natural sciences; Biological sciences; Neuroscience; Systems neuroscience

Kaminska et al., 2025, iScience *28*, 112313
May 16, 2025
https://doi.org/10.1016/j.isci.2025.112313

CellPress

iScience

CellPress
OPEN ACCESS

Article

Auditory evoked delta brushes involve stimulus-specific cortical networks in preterm infants

Anna Kaminska,[1,2,3,4,16,*] Dorothée Arzounian,[1,2,3] Victor Delattre,[1,2,3] Jacques Laschet,[1,2,3] Jean-François Magny,[5] Shushanik Hovhannisyan,[5] Mostafa Mokhtari,[6,7] Antoine Manresa,[8] Anne Boissel,[8] Lisa Ouss,[9] Lucie Hertz-Pannier,[1,2,3] Catherine Chiron,[1,2,3] Fabrice Wendling,[10] Yves Denoyer,[10,11] Mathieu Kuchenbuch,[12,13] Jessica Dubois,[1,2,3,15] and Roustem Khazipov[14,15]

[1]Inserm, UMR 1141 NeuroDiderot, Paris, France
[2]CEA, NeuroSpin, UNIACT, Gif-sur-Yvette, France
[3]Université Paris Cité, Paris, France
[4]AP-HP, Necker-Enfants Malades Hospital, Department of Clinical Neurophysiology, Paris, France
[5]AP-HP, Necker-Enfants Malades Hospital, Neonatal Care Unit, Paris, France
[6]Bicêtre Hospital, Neonatal Intensive Care Unit, Le Kremlin-Bicêtre, France
[7]AP-HP, Espace Ethique-Ile de France, CHU Saint-Louis, Paris X, France
[8]Laboratory CRFDP, University of Rouen, Normandy, France
[9]AP-HP, Necker-Enfants Malades Hospital, Child and Adolescent Psychiatry Unit, Paris, France
[10]INSERM, LTSI – U1099, University of Rennes, 35000 Rennes, France
[11]GHBS, Lorient, France
[12]Department of Pediatrics, Reference Center for Rare Epilepsies, University Hospital of Nancy, Member of ERN EpiCare, 54000 Nancy, France
[13]UMR 7039, CRAN, CNRS, University of Lorraine, 54000 Nancy, France
[14]INMED, INSERM, Aix-Marseille University, Marseille, France
[15]These authors contributed equally
[16]Lead contact
*Correspondence: anna.kaminska@aphp.fr
https://doi.org/10.1016/j.isci.2025.112313

SUMMARY

During the third trimester of gestation in humans, the auditory cortex displays spontaneous and auditory-evoked EEG patterns of intermittent local oscillatory activity nested in delta waves – delta brushes (DBs). To test whether the spatiotemporal dynamics of evoked DBs depends on stimulus type, we studied auditory evoked responses (AERs) to voice and "click" using 32-electrode EEG in 30 healthy neonates aged 30 to 38 post-menstrual weeks. Both stimuli elicited two peaks at approximately 250 ms and 600 ms, the second corresponding to the first principal components of the AER and the evoked DB. The DB showed stimulus-specific topography, temporal posterior and mid-temporal for "click", and mid-temporal and pre-central inferior for voice, and contained theta to gamma oscillations more widespread for the "click"response. Gamma oscillations increased with age. AERs predominated on the right but shifted toward the left with age for voice response. Auditory evoked DBs may therefore underlie specific auditory processing during fetal development.

INTRODUCTION

During early developmental stages (i.e., the third trimester of gestation in humans and the equivalent first ten-day postnatal period in rodents), the immature sensory cortex displays homologous patterns of activity in the form of intermittent local oscillatory activity bursts, namely delta brushes (DBs) in humans and spindle/gamma bursts in rodents.[1–5] This activity is characterized by short-lived fast oscillations in the alpha to gamma frequency range nested within the envelope of delta waves. Considerable evidence indicates that these early cortical activity patterns are largely driven by spontaneous activity at the sensory periphery: in the somatosensory cortex by sensory feedback resulting from myoclonic twitches, in the visual cortex by retinal waves, and in the auditory cortex by spontaneous cochlear activity.[5–13] Supported by these early patterns, correlated activity and synaptic plasticity in thalamocortical networks are thought to sustain the activity-dependent formation of somatotopic, retinotopic, and tonotopic cortical maps during the pre-critical and critical periods of thalamocortical development.[2,14–22] These early activity bursts can also be evoked in the corresponding sensory areas by sensory stimuli of different modalities including somatosensory, visual, and auditory, although with some interspecies and intersystem differences.[2,6–8,10,23–26] However, these

all-or-none sensory-evoked bursting responses, which involve high neuronal participation, seem incapable of conveying graded and high-frequency information transfer as in adults.[7,27] This raises the question of whether the spatiotemporal dynamics of these early bursting responses depend on the physical characteristics of the stimulus, which may underlie the ability to differentiate complex sensory stimuli and support the early emergence of cognitive abilities. This question is of particular importance for sensory signals in the auditory modality, which efficiently reach human fetuses in the womb, unlike visual stimuli. Behaviorally, auditory cognitive abilities emerge in humans during the fetal period and newborns already show remarkable behaviors from birth: they can recognize their mother's voice from prenatal exposure, they are able to discriminate between different sounds (speech, music, and combination of pure tones), and they can remember acoustic cues of a target passage of a story read prenatally.[28–32] The ability of premature newborns from 28 post-menstrual weeks (PMW) to discriminate between phonemes or between male and female voices has been demonstrated through the mismatch responses to phonetic and voice changes observed with functional near-infrared spectroscopy and high density electroencephalography (EEG).[33,34] Together, these findings indicate that the fetal brain is capable of discriminating patterned auditory stimuli including voice and nonverbal signals. However, the specifics of the cortical activity patterns providing the neurophysiological basis for these early abilities remain largely unknown.

Auditory evoked responses (AERs) are among the ontogenically earliest sensory EEG responses and display gradual developmental changes in the timing of all components between the immature and mature systems. Previously studied mainly through the event related potentials (ERPs) technique that average tens of stimulus-locked responses, AERs are not a unitary phenomenon but, rather, a series of temporally overlapping waves or components representing activity from various cortical and subcortical sources.[35]

The latencies and morphology of auditory ERP peaks are highly dependent upon the auditory stimulus: in particular ERP amplitude, latency, and scalp distribution can be manipulated by changes in stimulus rise time, duration, inter-stimulus interval, level (intensity), complexity, and tone burst frequency.[36,37] Brain processes associated with detection, discrimination, and developmental plasticity can therefore be investigated using scalp-recorded AERs. Previous studies using standard (9-electrode) EEG recordings in healthy preterm newborns revealed that both vocal and click stimuli evoke AERs with a prominent late component of DB in the temporal cortex which reaches maximal amplitude before the age of 35 PMW and vanishes at full term (~40 PMW).[23] More recently, using 32-electrode EEG recordings in healthy neonates from ages 30 to 38 PMW, we showed that click-evoked DBs occur in temporal regions, include oscillatory activity from delta to gamma frequency bands, and correspond to the late component of AERs and auditory ERPs peaking around 500–700 ms.[8]

To test whether the auditory evoked DBs, represent stimulus-specific features, we aimed to perform comparative analyses of AERs, including their late component of DBs, after two physically different auditory stimuli (voice and "click") in the same population of 30 healthy neonates aged 30–38 PMW, using the same recording setting.[8] We performed visual, spectral power density, power spectrum (PS) and time-frequency (T-F) analyses allowing study of event-related spectral perturbations (ERSPs). We used averaging and principal component analyses (PCA) to study the morphology of auditory ERPs. These complementary analyses allowed to dissect spectral components of AERs including their late DB component. We compared DB response rates after both stimuli; auditory ERPs (identification of peaks, their amplitude, latency and scalp topography) and AER oscillatory components using visual, PS and T-F analyses. Finally, we assessed the developmental course of AERs between 30 and 38 PMW.

RESULTS

"Click" evoked visually identifiable DBs better than voice (in 83 versus 50% of babies)

Vocal stimulus (a spoken word "bébé", meaning "baby" in French) evoked DBs at the mid-temporal (T7-T8) and pre-central inferior (FC5-FC6) electrodes, peaking at around 500–700 ms and preceded by a theta band sharp peak culminating at the FC5-FC6 electrodes at around 250 ms (see Figures S1 and 1A). As previously described[8] "click" evoked DBs mostly on the mid-temporal (T7- T8) and temporal-posterior (CP5-CP6) electrodes, also peaking at around 500–700 ms and also preceded by a negative sharp peak in the theta band visible on the FC5-FC6 electrodes (Figure 1A). Spontaneous DBs at temporal electrodes had similar aspect but were not preceded by the small initial theta component (Figure 1A). Voice evoked visually identifiable DBs (response rate >10%) in 50% of infants (15/30), encompassing the 3 age groups but only 3 infants among the youngest had easily identifiable DBs (response rate >30% compared to 20–30% in the other 12 patients) (see Table S1). In contrast, and as previously reported, "click" evoked visually identifiable DBs in 83% of infants (25/30), more than voice presently did ($p < 0.01$), and were easily identifiable in 50% of babies (15/30).[8]

Voice- and "click"-evoked ERPs differ mainly in the topography of late DB component

Considering individual and group-level AER averaging, we observed that auditory ERPs showed two distinct negative peaks for both stimuli. The first peak (N1) had a sharp waveform and was located at approximately 250 ms latency. The second peak (N2) was at around 500–700 ms, it had a vast and shallow waveform of around 20 μV amplitude with double polarity: negative at the pre-central inferior (FC5-6), mid-temporal and temporal posterior (T7-8, CP5-6) electrodes and corresponding to the visually observed DBs, and positive polarity at the midline Fz, Cz, Pz and POz electrodes (Figures 1B and 1C; Figures 2A, 2B, and 2C; Figure 3A). N2 was followed by a vast positivity at CP5-6 and T7-8 electrodes peaking at around 1500–2000 ms (Figure 3A). Group-level analyses ($n = 30$) showed significant differences between voice and "click" evoked ERPs in terms of spatial distribution and amplitude of peaks (Figures 3B and 3C, see also Video S1). "Click" evoked an N1 peak on the T8, CP6 and CP5 electrodes as well as an N2 peak on CP5 and CP6 of higher amplitude than voice did. In contrast, voice evoked an N2 peak on FC5 and FC6 of higher amplitude than "click" did (Figures 3B and 3C, see

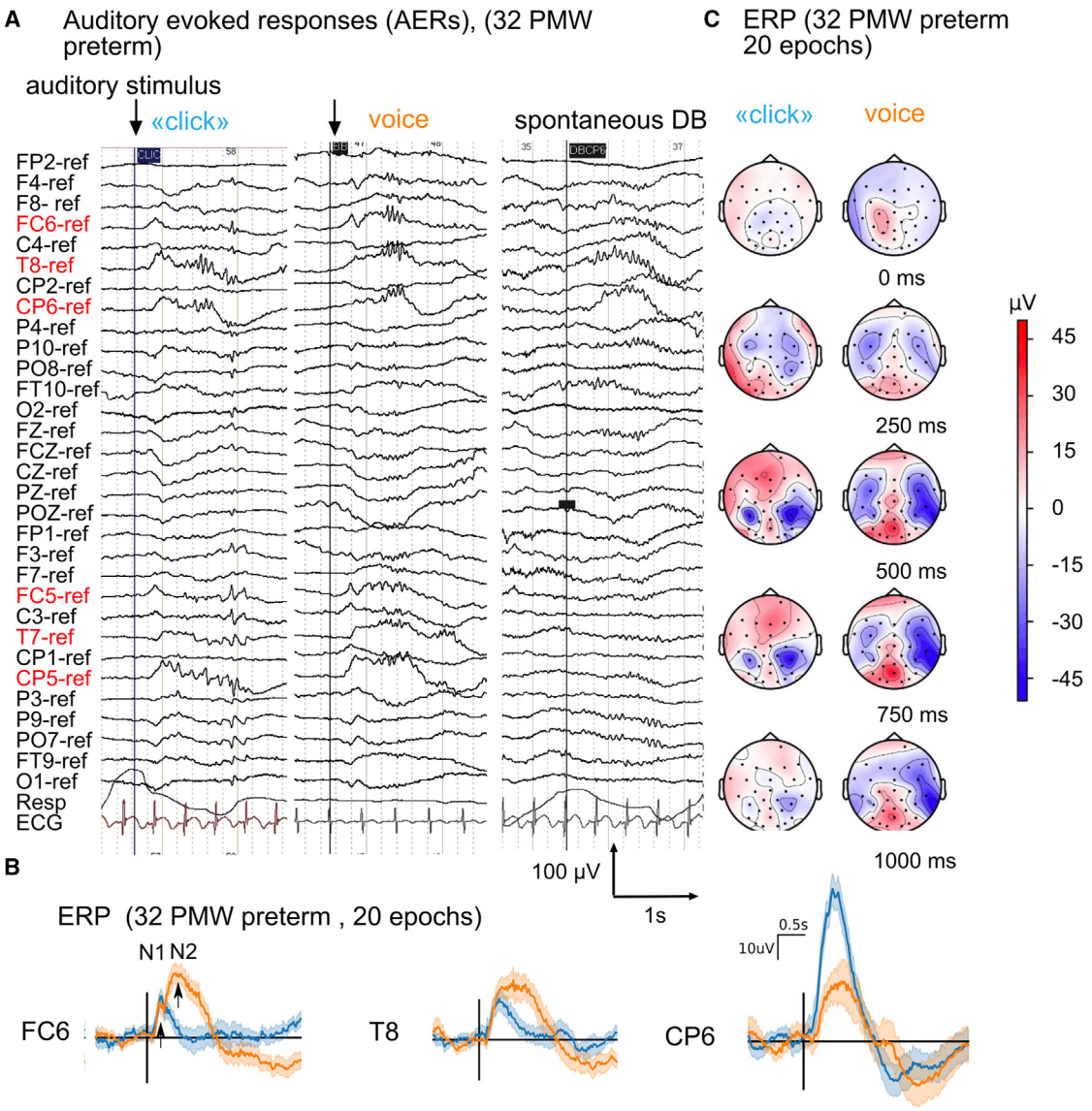

Figure 1. Visual inspection of the auditory click and voice-evoked responses (AERs) in a 32 post-menstrual weeks (PMW) preterm neonate

(A) EEG with average reference (high pass filter: 0.16 Hz, notch filter: 50 Hz, upward deflection represents negative potential) in a 32 PMW preterm showing (from left to right) representative examples of AERs including delta brushes (DBs) evoked by auditory stimuli "click" and the spoken word "baby" on the T7, T8, CP5, CP6, and FC5, and FC6 electrodes as well as spontaneous DBs on the T8, CP6 and FC6 electrodes. Note the right predominance of evoked DBs.

(B) Average auditory event related potentials (ERPs) after the "click" (blue) and voice (orange) stimuli in the same preterm on target electrodes showing the main evoked DBs responses (CP6, T8, FC6). Two black arrows depict the apparent location of distinct peaks, N1 and N2 contributing to the auditory ERPs. Shaded area, SEM.

(C) Color maps of spatial distribution of "click" and voice evoked ERPs at different delays after the stimulus onset in the 32 PMW preterm.

also Video S1). Since stimuli were presented non-randomly, we performed a statistical comparison of epochs averaged over the first 5 and the last 5 presentations of each stimulus type in order to detect a potential presentation order bias. We found no difference in the AERs between the start and the end of the stimulation protocol (Figure S2). Considering individual AER averaging, a subgroup of 9 babies had identifiable ERP after both stimuli (30–33 PMW: n = 3; 34–38 PMW: n = 6), which were further used to compare ERP latency and amplitude across stimuli (see Table S2 and Figure 4A). The latencies of N1 and N2 peaks after "click" and voice were comparable on corresponding electrodes (N1 on FC5-FC6 (252 ± 27 ms, and 257 ± 53 ms (mean ± SD), N2 on T7-T8 (394 ± 87 ms and 495 ± 184 ms) and N2 on CP5-CP6 (558 ± 125 ms and 563 ± 196 ms) respectively (non-significant). No age group differences were observed for N1 and N2 peak latencies for "click" nor voice (Figure 4B, see Table S2).

Comparing peak amplitude after both stimuli, the N2 peak on CP5-6 had higher amplitude after "click" (24 ± 12 µV) than after

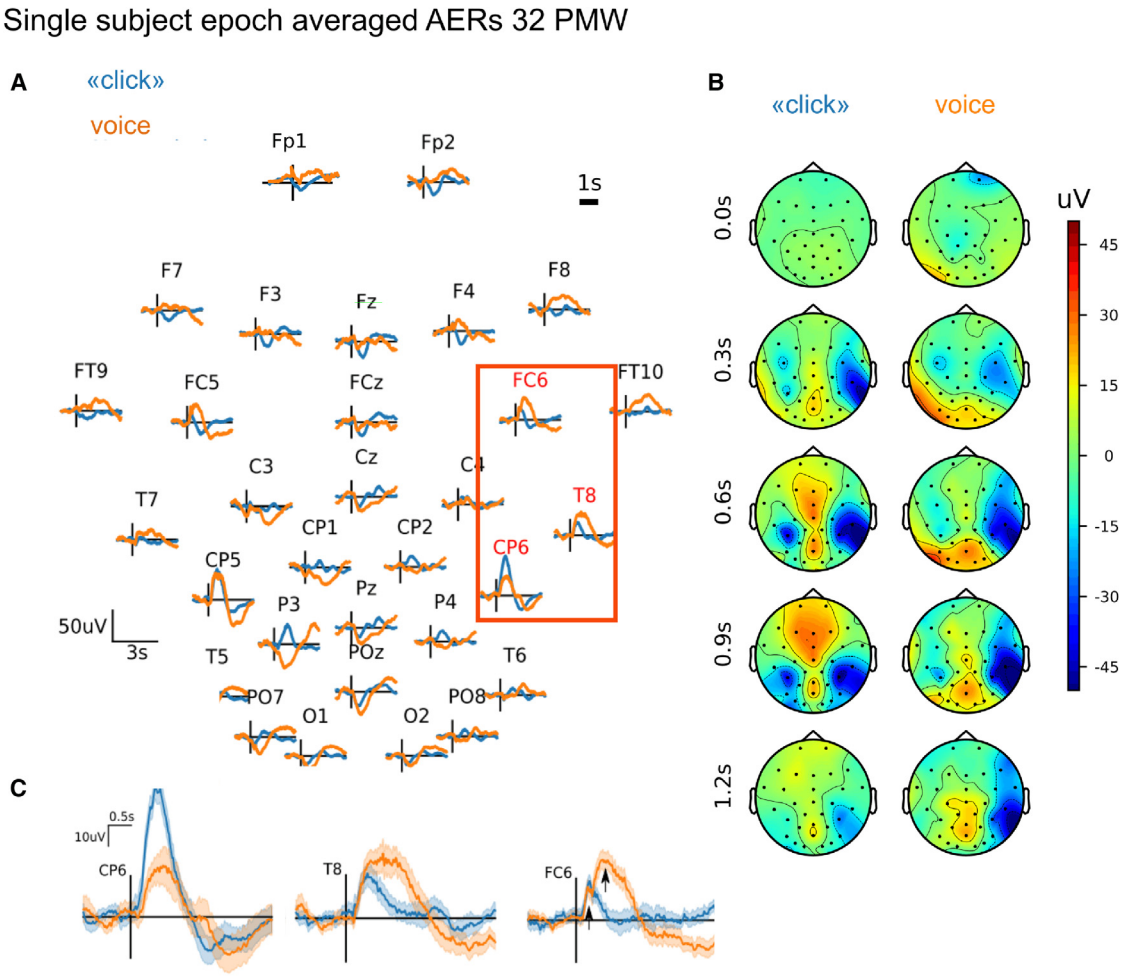

Figure 2. Click and voice auditory event related potentials (ERPs) in a 32 PMW infant

(A) Surface plot of epoch-averaged AERs (n = 23 for vocal and n = 71 for "click" stimuli), electrodes marked in red (in rectangle) are considered in detail in C.

(B) corresponding 2D maps at 300, 600, 900 and 1200 ms after the stimulus onset.

(C) Zoom on ERPs for target right electrodes (CP6, T8, and FC6). Thick lines depict average and semi-transparent regions standard error of the ERPs.

voice (16 ± 10 μV; $p < 0.05$) while the amplitude of N2 on T7-T8 was similar after both stimuli. For "click" and voice, the N2 amplitude was significantly lower on CP5-CP6 at 34–38 PMW than at 30–33 PMW ($p < 0.05$ and $p < 0.001$ respectively). The age-related difference in N2 amplitude was also observed on T7-T8 after voice ($p < 0.05$) (see Table S2; Figure 4B).

Principal component analysis (PCA) of voice and "click" ERPs at group-level (n = 30) was first performed including 31 electrodes. The first PC of "click" and voice ERPs explained 90% and 72% of variance respectively and corresponded to a slow negative delta wave peaking around 500–700 ms (see Figures S3A and S3B). Highest absolute values of PC1 scores corresponded to CP6, CP5, and T8 for "click" and the T8, POz, FC6, and FC5 electrodes for voice respectively (see Figures S3A and S3B). PC1 corresponded therefore to the N2 peak as disclosed by ERPs analyses, the negative delta component of the evoked DBs.

The PCA of epoch-averaged AERs performed on target electrodes as described above and showing the highest ERPs amplitude and main power spectrum increase (T7-8, CP5-6, FC5-6)[8] showed that PCA did extract N1 and N2 peaks among the first two principal components (PC2 and PC1respectively). PC1 and PC2 explained variance ratios of 44% and 16% respectively, which by themselves could discriminate ERPs to voice and "click" with 80% accuracy (Figures 5A and 5B). The activation maps of these first two principal components confirmed a clear difference in their anterior-posterior topography (Figure 5C). The first component (PC1) coincided with the late N2 peak; it was dominant on the left pre-central inferior electrode (FC5) after voice and on the mid-temporal and temporal posterior electrodes (T7, T8, CP5, and CP6) after "click", while the second component (PC2) with a peak coinciding with the early N1 peak was dominant on FC5 and FC6 after "click" only (Figure 5C).

When assessing PC1 and PC2 differences between the two previous age groups (30–33 PMW: n = 3; 34–38 PMW: n = 6), only the late component (PC1) on FC6 after voice revealed a significantly lower amplitude in older subjects (0.02 ± 0.35) than younger subjects (1.35 ± 0.21) ($p < 0.05$).

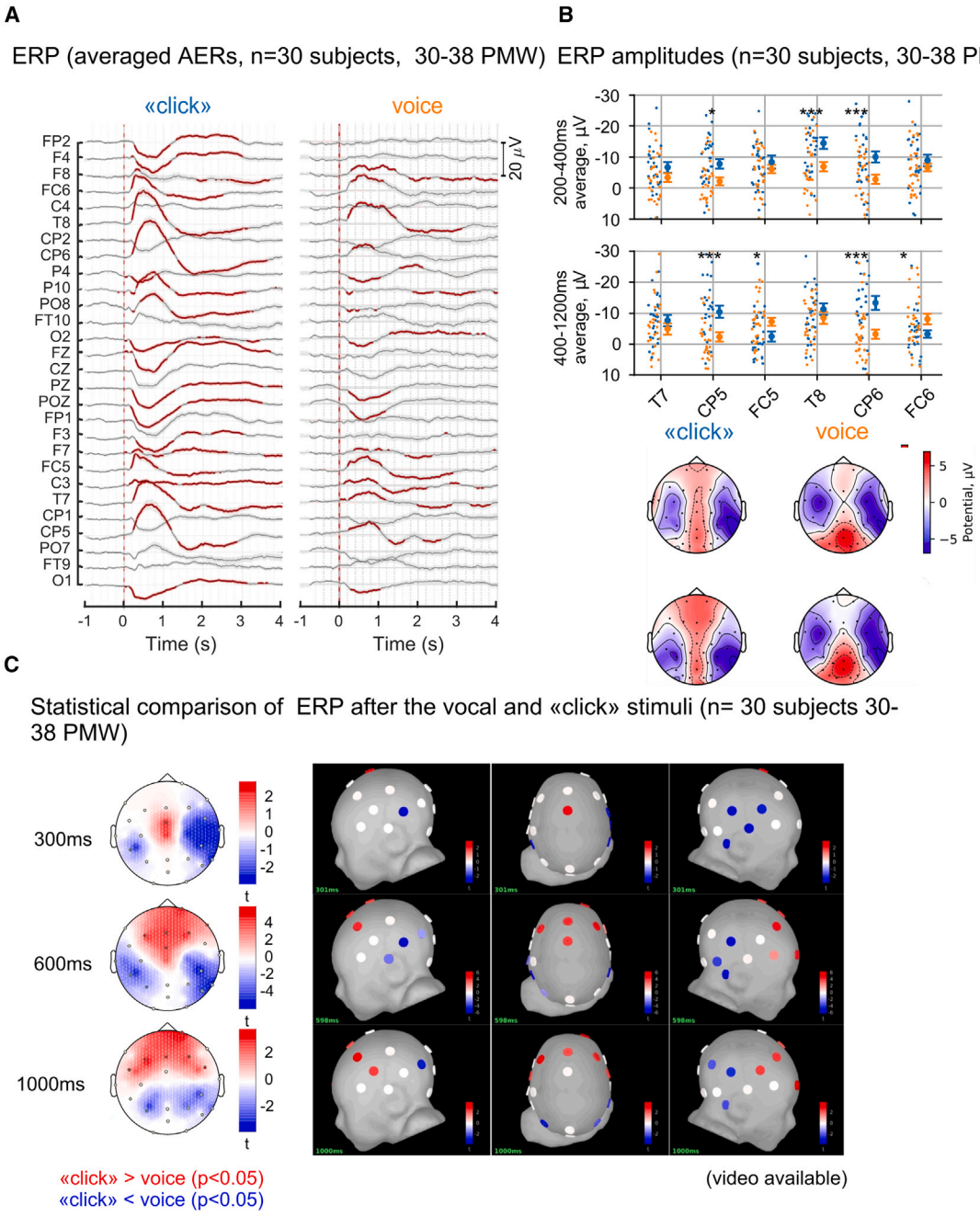

Figure 3. Click and voice auditory event related potential (ERP) topography (*n* = 30 subjects)

(A) Grand average ERPs (*n* = 30 subjects) evoked by "click" and voice auditory stimuli. The red-highlighted portions indicate significant deflections from the 200 ms prestimulus baseline.

(B) Each dot represents single subject ERP amplitude (*n* = 30 subjects) for the time windows of the N1 (200–400 ms) and N2 (400–1200 ms) peaks for "click" (blue) and voice (orange) stimuli at selected electrodes (above) and the corresponding color maps (below). Thick lines depict average and SEM of the group (*n* = 30 subjects, 30–38 PMW). Asterisks indicate significant differences between stimulus types at the group level (* <0.05, ** <0.01, and *** <0.001, Student's *t* test).

(C) Student's *t*-statistics of the voice versus "click" analysis, for significant clusters of a cluster-based permutation test with $p < 0.05$ threshold. Red color depicts regions where "click" ERPs are more positive than voice ERPs; blue depicts regions where "click" ERPs are more negative than the voice evoked ones. The figures are drawn for 3 time points of interest: 300 ms, 600 ms and 1000 ms after the stimulus onset.

See also Video S1.

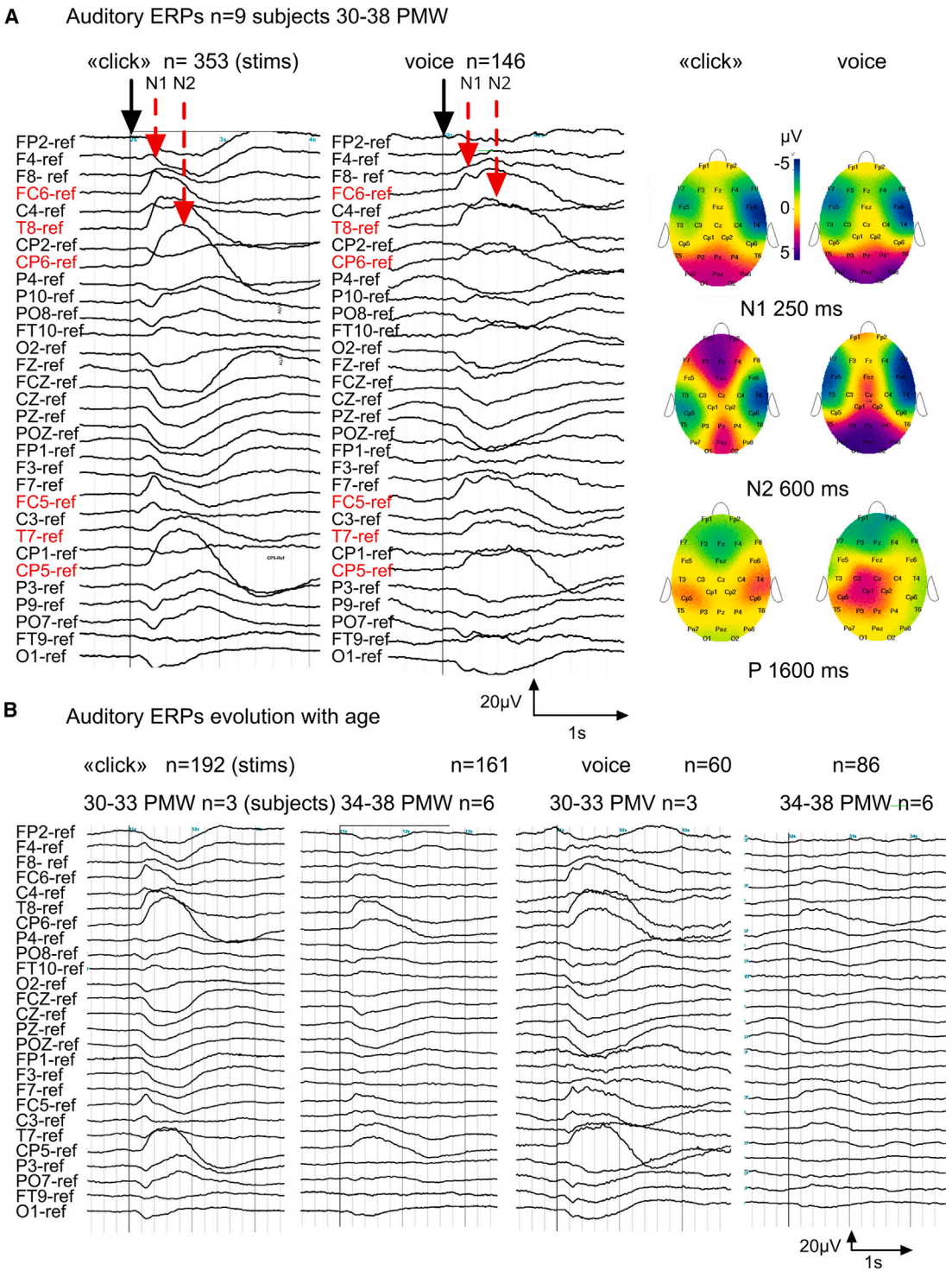

Figure 4. Auditory event-related potentials (ERPs) evoked by click and vocal stimuli and age related development showed in a subgroup of 9 subjects who had identifiable ERP after both stimuli

(A) "Click" (left) and vocal (right) stimuli group locked averaging (n = 9 subjects). Averaged waveforms are represented on 31 EEG electrodes using a 0.16 Hz high pass filter and mean reference (upward deflection represents negative potential). On the right averaged waveforms are represented on 2D EEG mapping (Coherence software), locked to the positions N1 (250 ms) and N2 (600 ms) as defined by the time cursor (red arrows) and 1600 ms corresponding to the peak of a large positivity at CP5 and CP6 electrodes after "click".

(B) Age related development of ERPs after "click" and vocal stimuli in a group of 30–33 PMW (n = 3) and of 34–38 PMW (n = 6) subjects.

See also Table S2.

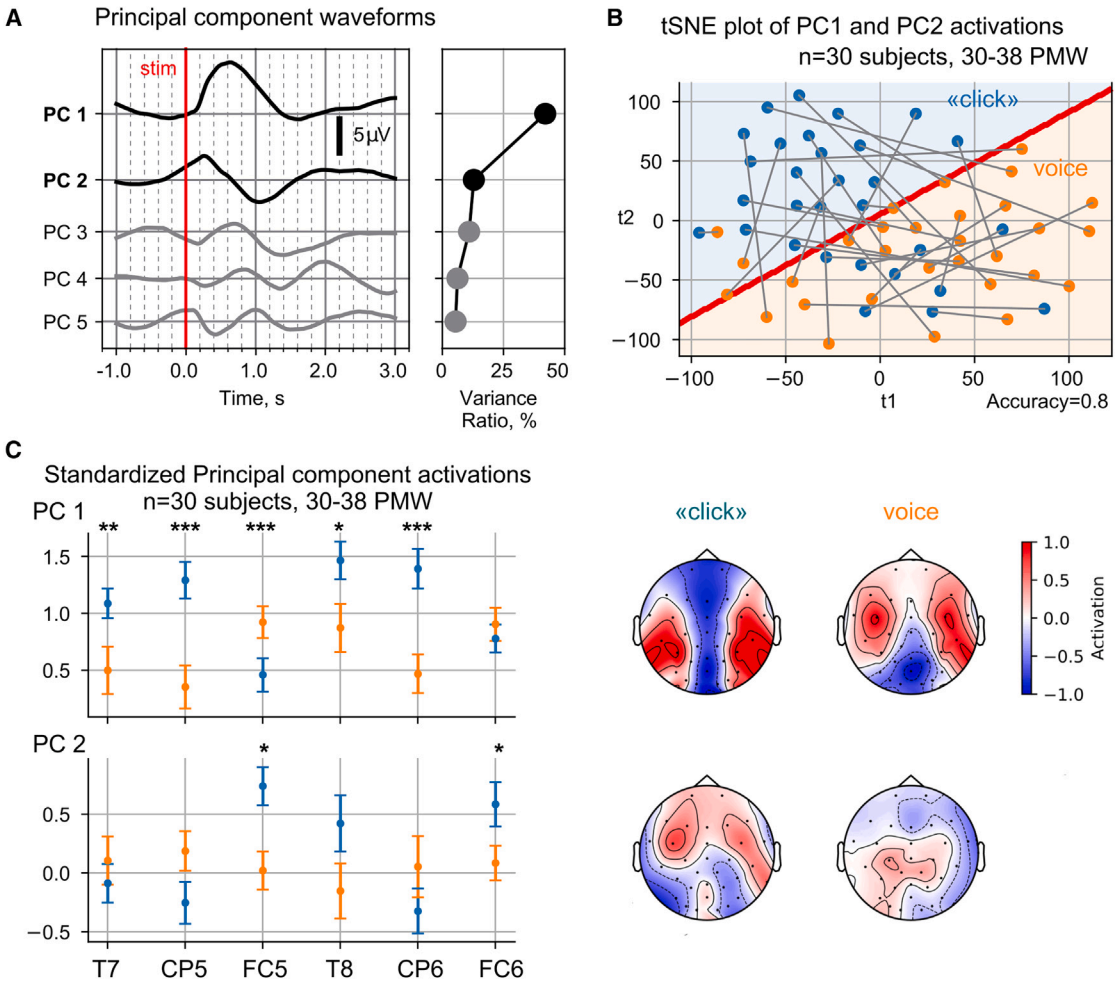

Figure 5. Principal component analysis (PCA) of click and voice ERPs

(A) The first five principal components (PCs) of the ERPs (left) and their variance ratio (right) (n = 30 subjects). The two peaks at 250 ms and 600 ms are represented by the first two components PC1 and PC2, respectively. PC1 and PC2 cover 55% of the total variance.

(B) A render of a planar tSNE transform (t1, 2) of PC1 and PC2 for all electrodes in all subjects. Each subject is represented by a pair of connected dots. A blue dot corresponds to the projection of the "click" ERPs and an orange dot to the projection of the voice evoked ones. The two apparent clusters for voice and "click" ERPs tend to segregate with an accuracy of 0.8 suggesting that PC1 and PC2 are sufficient to discriminate ERPs evoked by both stimuli. The red line represents a discriminative plane reconstructed with a supporting vector machine classifier.

(C) Group analysis of the PC1 and PC2 activation on selected electrodes (left) and the corresponding PC activation maps (right). The component activations were standardized channel-wise for each subject. Markers depict group average and whiskers – group standard errors (n = 30 subjects, 30-38G PMW). Asterisks indicate significant differences in the group (*< 0.05, **< 0.01, and ***< 0.001, Wilcoxon signed-rank test).

AERs after both stimuli contain delta to gamma band oscillations

Group-level power spectrum (PS) analyses (n = 30) showed that voice induced a significant post-stimulus power increase in the theta to beta bands on the right pre-central inferior (FC6) and the right mid-temporal (T8) electrode (p < 0.01) and in high-gamma power on the right pre-central inferior (FC6) electrode (p < 0.01) (Figure 6A, see Table S3). In contrast, "click" induced a significant increase of power in frequency bands ranging from delta to beta at most electrodes (p < 0.01 and p < 0.001, one-tailed paired Student's t-tests) (Figure 6A, see Table S3). We also observed a click-related increase in the gamma band (30–80 Hz) power on the frontal mesial (Fz) and right mid-temporal and temporal posterior (T8 and CP6) electrodes (p < 0.01), as well as in high-gamma (>80 Hz) power on the right temporal posterior (CP6) electrode (p < 0.01) (Figure 6A see Table S3). Comparing the PS increase (Δ Log PS) (Log transform of power spectrum increase = Δ Log PS= (Log PS′ 2s after stim′) - (Log PS′ 2s before stim′) between both stimuli, we found a significantly higher Δ Log PS on most electrodes in the delta to beta bands after "click" (p < 0.05). However, voice induced higher responses in gamma and high-gamma power on FC6, F4, CP2 and C3 (p < 0.05) (Figure 6B, see Table S4). Spontaneous DBs visually identified on the T7-8 and CP5-6 electrodes, selected in all subjects, showed a significant increase of

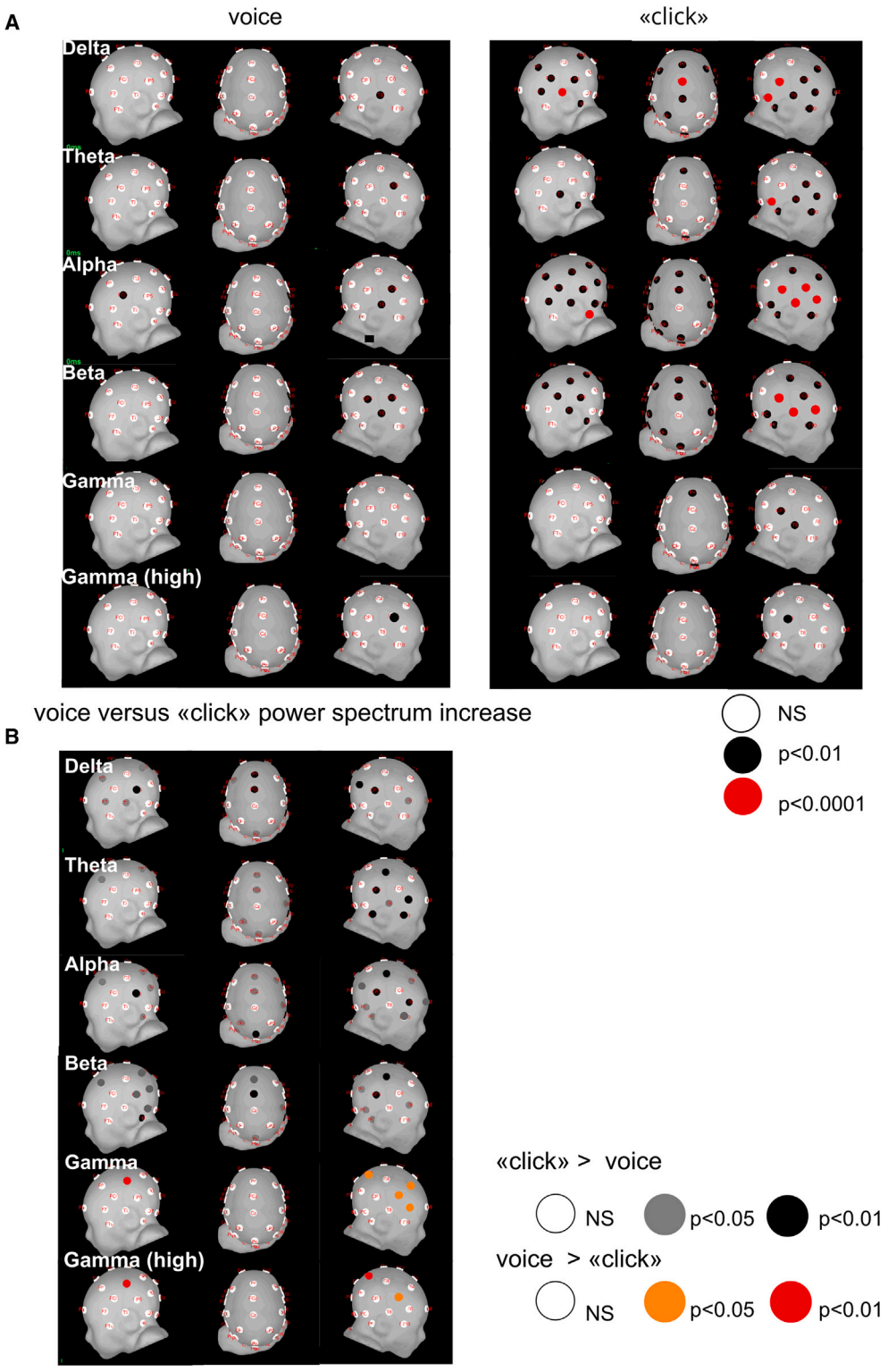

(legend on next page)

power in delta to gamma in the frequency band of 0.5–48 Hz (not tested for gamma >48 Hz).

Time-frequency (T-F) group level (n = 30) analysis in the 1–45 Hz frequency band with an equivalent number of epochs after both stimuli showed significantly positive ERSPs after "click", corresponding to an increase in oscillation amplitude compared to the pre-stimulus baseline, at frequencies spanning delta to gamma bands and on most electrodes ($p < 0.05$), but with the widest time-frequency span on FC5-6, T7-8, and CP5-6 (Figure 7A). In contrast, voice evoked localized and weak theta to beta band oscillations on the pre-central inferior (FC5-6) and right mid-temporal (T7-8) electrodes (Figure 7B). Comparing ERSP maps across stimulus types revealed significantly stronger beta oscillations on both CP6 and CP5 as well as stronger gamma oscillations on CP6 after "click" compared to voice (Figure 7C).

Group level (n = 30) T-F analysis covering a larger frequency band including high-gamma (10–120 Hz) and focused on the target FC5-6, T7-8, and CP5-6 electrodes, revealed significantly positive ERSPs corresponding to an increase in oscillation amplitude compared to the pre-stimulus baseline after the "click" at frequencies spanning from alpha up to 120 Hz ($p < 0.05$) (Figure 8A, left). Voice also evoked identifiable ERSPs in the gamma band (Figure 8B, left). T-F maps after "click" showed an inter-trial coherence (ITC) up to 0.25 in the delta to beta band in two temporal intervals, one centered around 200–300 ms and one later varying slightly across electrodes (from 500 to 1000 ms on FC5-FC6 and T7-T8 and from about 750 to 1250 ms on CP5-CP6) coinciding with the time windows of N1 and N2 ERPs peaks respectively (Figure 8A, right). ERSPs after voice showed a different pattern of ITC peaking at three latencies around 200, 500 and 1000 ms on FC5-FC6 and mainly around 200 ms on T8 and CP6 (Figure 8B, right).

Visual inspection of individual raw EEGs, spectral power density, and wavelet analyses (Natus-Coherence review program) confirmed the presence of well-individualized oscillatory response in the gamma band mainly in the time window between 200 ms and 1.5 s after the stimulus onset (Figures 9A and 9B). Gamma oscillations in the frequency range of 30–40 Hz were visually identifiable within AERs after "click" and voice and on spectral power density analyses of single AERs or after averaging the power spectra on 2 s epochs before and after the stimulus onset (Figure 9C). In contrast, oscillatory activity in the high-gamma band (>80 Hz) was not distinguishable from the background activity which contained frequent environmental powerline and EMG artifacts.

The spectral power increase after both stimuli predominated in the right hemisphere, but shifted toward the left with age after voice

Evaluating inter-hemispheric AER asymmetries comparing ΔLog PS among electrodes with significant Log PS increase after auditory stimulus, we found larger ΔLog PS on the right side after voice on the pre-central inferior (FC5-FC6; $p < 0.001$) and mid-temporal (T7-T8, $p < 0.05$) electrodes. After "click" there was also a right predominance of PS increase on mid-temporal (T7-T8) and temporal posterior (CP5-CP6) electrodes ($p < 0.0001$) (see Table S5). The effect of gestational age (as a continuous variable in PMW) on lateralization, assessed by a slope F-test after linear regression of the difference between responses (ΔLog PS) of each homologous electrode pair versus age, showed that the right predominance of evoked PS on pre-central inferior (FC5-FC6) and mid-temporal (T7-T8) and temporal posterior electrodes (CP5-CP6) pairs after voice shifted to the left with age ($p < 0.05$) (See Table S5). Using multivariate analyses of the PS increase after both stimuli and during spontaneous DBs on the right temporal (T8 and CP6) electrodes we found that "click" induced 2 widespread dominant clusters, mainly in the delta to alpha bands on the vertex, central, frontal and temporal electrodes whereas voice induced localized clusters on the frontal, central and temporal electrodes (Figure S4). Spontaneous T8 DBs disclosed a large and bilateral first cluster on the central-parietal, occipital and temporal posterior electrodes in the gamma band (Figure S4). Overall, AERs to voice and "click" and spontaneous DBs showed different PS-based clustering and some gain in topological complexity, i.e., smaller and more numerous clusters when comparing voice to "click" evoked AERs.

Evoked power in the delta to gamma band increased across gestational age

Analyzing PS increase and including all electrodes as independent variables and age as continuous variables (multiple linear regression model (least squares fitting), we showed an effect of electrodes on PS after "click" ($p < 0.001$) and voice stimulus ($p < 0.01$) and an effect of age ($p < 0.00001$) for both stimuli, whatever the frequency band. After "click", PS increased with age in all frequency bands including gamma on the right temporal posterior electrodes (CP6) ($p < 0.05$) and on the left temporal posterior basal electrodes (P9) ($p < 0.05$) (Figure S5, see Table S6). Responses also increased with age on the right mid-temporal (T8) (in the theta to beta bands), left mid-temporal (T7) (in delta to alpha bands), and left temporal posterior (CP5) (in delta, alpha and beta bands) electrodes ($p < 0.05$). PS decreased with age on vertex (CZ) electrode (in theta to beta bands). After

Figure 6. Frequency power spectrum (PS) analysis of auditory evoked responses (AERs) after voice and click stimuli (n = 30 subjects) (Student's paired t tests) and comparison of PS increase after both stimuli

(A) The frequency power spectra of mean-referenced signals were computed over 2-s time intervals using the Fast Fourier Transform algorithm and spectra immediately preceding and following auditory stimuli were compared in 6 frequency bands (delta = 0.5–3.5 Hz; theta = 4.0–7.5 Hz; alpha = 8.0–13.0 Hz; beta = 13.5–29.5 Hz; gamma (30–48.0 Hz and 52.0–80.0 Hz) and high-gamma (80.5–98.0 Hz; 102.0–148.0 Hz and 152.0–198.0 Hz) (for details see STAR Methods section and Table S3). The significant increase of PS on a group-level analysis (n = 30 subjects) was represented for the values of $p < 0.01$ (black circle) and $p < 0.001$ (red circle) (one-tailed paired Student's t test for the difference between pre-and post-stimulus Log PS).

(B) Comparison between frequency PS increase (Log transform of power spectrum increase = Δ Log PS= (Log PS' 2s after stim') - (Log PS' 2s before stim') of auditory evoked responses (AERs) after "click" and voice stimuli (n = 30 subjects). Black ($p < 0.01$) and gray ($p < 0.05$) circles represent significant difference with higher Δ Log PS after "click" when compared to voice; while colors show significantly higher Δ Log PS after voice (one tailed paired Student's t test; red: $p < 0.01$; orange: $p < 0.05$, see also Table S4).

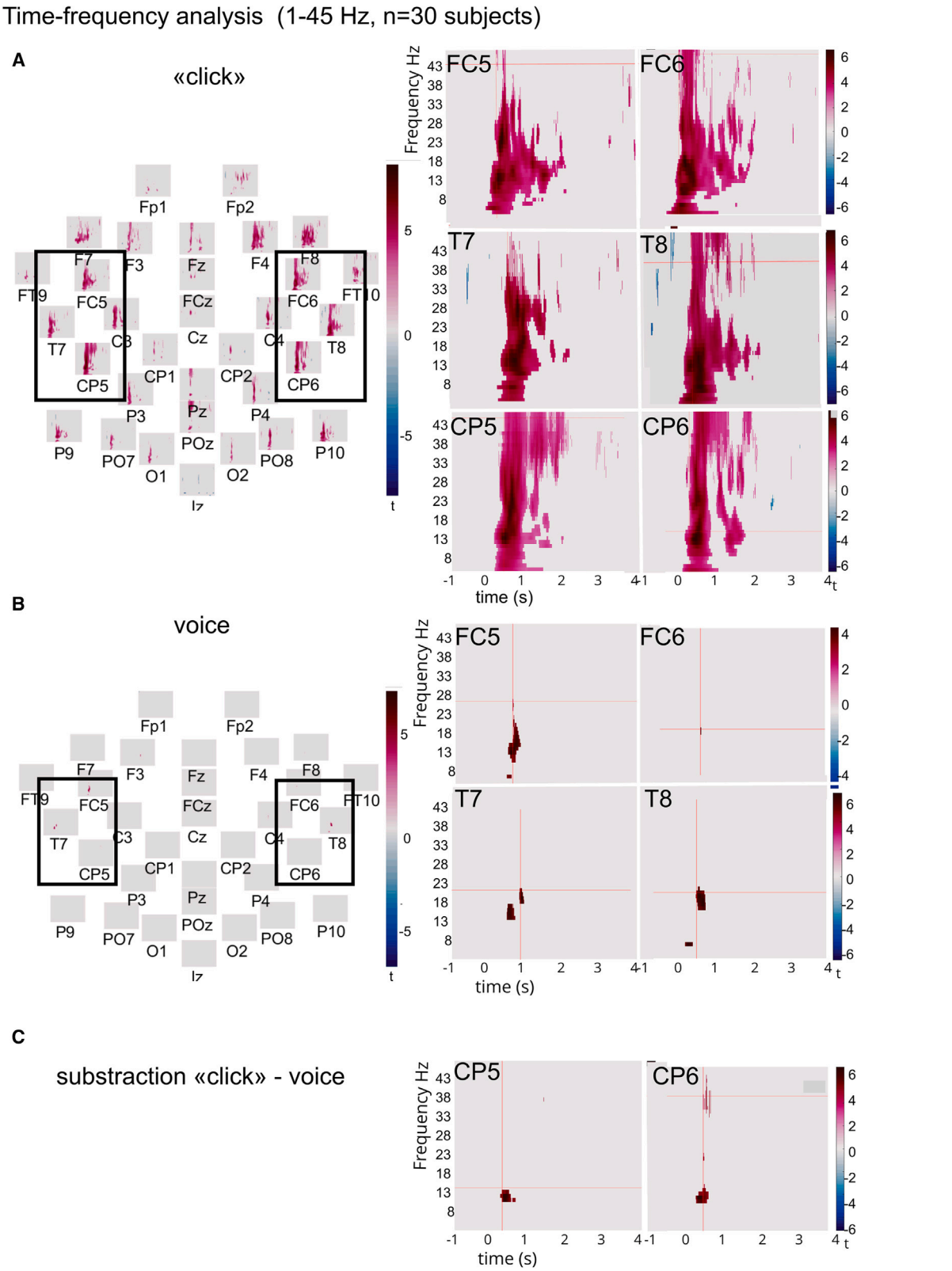

(legend on next page)

voice, PS increased with age in frequency bands ranging from delta to beta on the right mid-temporal (T8) and in theta and beta bands on left mid-temporal (T7) electrodes ($p < 0.05$). On the left and right pre-central inferior (FC5, FC6) electrodes PS increased in the alpha and beta bands respectively ($p < 0.05$) (Figure S5, see Table S6). It is of note that gamma oscillations within spontaneous DBs also increased with age on the T8 and CP6 electrodes ($p < 0.001$) (not tested for high-gamma).

When considering all electrodes, after voice, the whole model showed a trend of an increase in gamma power with age ($p < 0.001$), whereas responses after "click" decreased with age in the delta to alpha frequency bands power ($p < 0.01$). T-F analysis in the three age groups showed a trend to an increase of evoked spectral power density in the gamma band with age after "click" while this was not detectable on T-F analysis for voice (Figures S6 and S7).

DISCUSSION

Here, we revisited AERs in preterm humans, including their late DB component, analyzing them in frequency bands from delta to gamma and testing the hypothesis that these AERs share stimuli-specific profiles. Comparing ERPs after "click" and voice, we report significant differences mainly in the topography and amplitude of the evoked DBs. ERSPs also differ after both stimuli and display maturational changes during the age equivalent to the third gestational trimester: increased delta to beta and delta to gamma power in the mid-temporal and posterior regions respectively after "click" and in the mid-temporal and pre-central inferior regions after voice. AERs to both stimuli predominate on the right hemisphere but those to vocal stimuli will later shift to the left. Such stimulus-dependent spatiotemporal propagation patterns and oscillatory profiles of AERs reflect differential processing of auditory signals in specific cortical networks and likely contribute to the emergence of cognitive auditory abilities in the human fetus.

Auditory ERPs

Both stimuli result in the characteristic negative biphasic pattern previously reported for tones and clicks in preterm infants, whose late peak (N2, up to 700 ms) corresponds to the evoked DB and which vanishes near full term.[8,23,38] But AER averaging and PCA permit detection of higher N2 amplitude and stronger N2-related PC1 in temporal posterior for click and in pre-central inferior for voice. Latencies and amplitudes are in line with previously described normative studies of auditory ERPs in preterm, keeping in mind that N2 could not be recorded in these studies because of the absence of a temporal electrode and high-pass filtering too restrictive for the delta wave.[39] However, we found a similar latency and developmental profile of the N1 peak on FC5-FC6 to the so called "N2p" peak at around 250 ms on C3-C4 using ear ref.[8,39] Our auditory ERPs are also comparable regarding amplitude and latency to the preterm visual (VEPs) and somatosensory evoked potentials (SEPs) already reported by Hrbek et al. (negative peaks II and IV in VEPs and N2 and N3 in SEPs), with the evoked DBs as their late component.[6–8,38,40] A longer latency of AERs components is thought to reflect a higher stage of stimulus processing, involving associative auditory cortex and cognitive activity, thus higher-level sensory integration.[38,41,42]

Preterm cortical AERs underlie EEG oscillations dependent on the physical characteristics of the stimulus

We show here in preterm infants that AERs including their late component of DBs underlie EEG oscillations that differ according to the physical characteristics of the stimulus. Oscillations were spatially widespread for "click" and anteriorly focused for voice, with stronger right-lateralized responses for both stimuli but that shift to the left with age for voice, suggesting stimulus-specific cortical generators and information encoding by these oscillations. Similar to our findings several functional studies (f-MEG, ERP, NIRS) showed predominantly right responses for vocal stimuli starting from the third trimester of pregnancy (28–35 PMW), thus suggesting that right functional cortical maturation for auditory processing takes place early.[33,38,41,43,44] It is now well established that language networks are left lateralized in the brain from the very first months of life, with efficient perisylvian speech perception networks similar to those in adults.[45] But there is also growing evidence that these speech networks start to develop and become operational during the last trimester of fetal life.[46] In resting-state fMRI the perisylvian regions of this primordial language network appear bilateral before 30 GWA and subsequently left-lateralized.[47] Language brain structures and their connectivity develop from 20 PMW, these structures include the sylvian fissure, insula, superior frontal sulcus, inferior frontal gyrus, superior temporal sulcus and gyrus, superior longitudinal fasciculus and arcuate fasciculus.[46] In fMRI studies in children, passive listening of words activates the primary auditory cortex, superior temporal gyrus bilaterally, and left inferior frontal gyrus.[48] In fMRI studies, speech stimuli elicit significantly greater activation than both complex and simple non-speech stimuli in classic receptive language areas (mid-temporal gyri, left posterior superior temporal gyrus and right inferior frontal gyrus).[49] In our study "click" evoked DBs were located in mid- and posterior-temporal regions; the more anterior location of the voice-evoked DBs in pre-central inferior and their shift from right to left with age suggest the involvement of language networks in the generation of these DBs. However, our vocal and "click" stimuli were not normalized for intensity, duration nor acoustic frequency spectrum; their physical characteristics such as rise time and spectral content (narrow-band and peaking at 400 Hz for the vocal stimulus versus broad-band for the non-filtered "click") could potentially account for the differences in amplitude

Figure 7. Group-level ($n = 30$ subjects) time-frequency analysis of auditory evoked responses (AERs) (in 1–45 Hz)

"Click" (A) voice (B) stimuli, and comparison between both stimulus types (C). Colors represent t-statistics after application of a significance threshold mask ($p < 0.05$ corrected for multiple comparisons across time, frequency and channel dimensions, using the false discovery rate method). A-B Red corresponds to significantly positive event-related spectral perturbation (ERSP), that is, to a significant increase in power relative to the pre-stimulus (from −1500 to 4000 ms) baseline. (C) Red corresponds to a significantly positive "click" – voice ERSP difference.

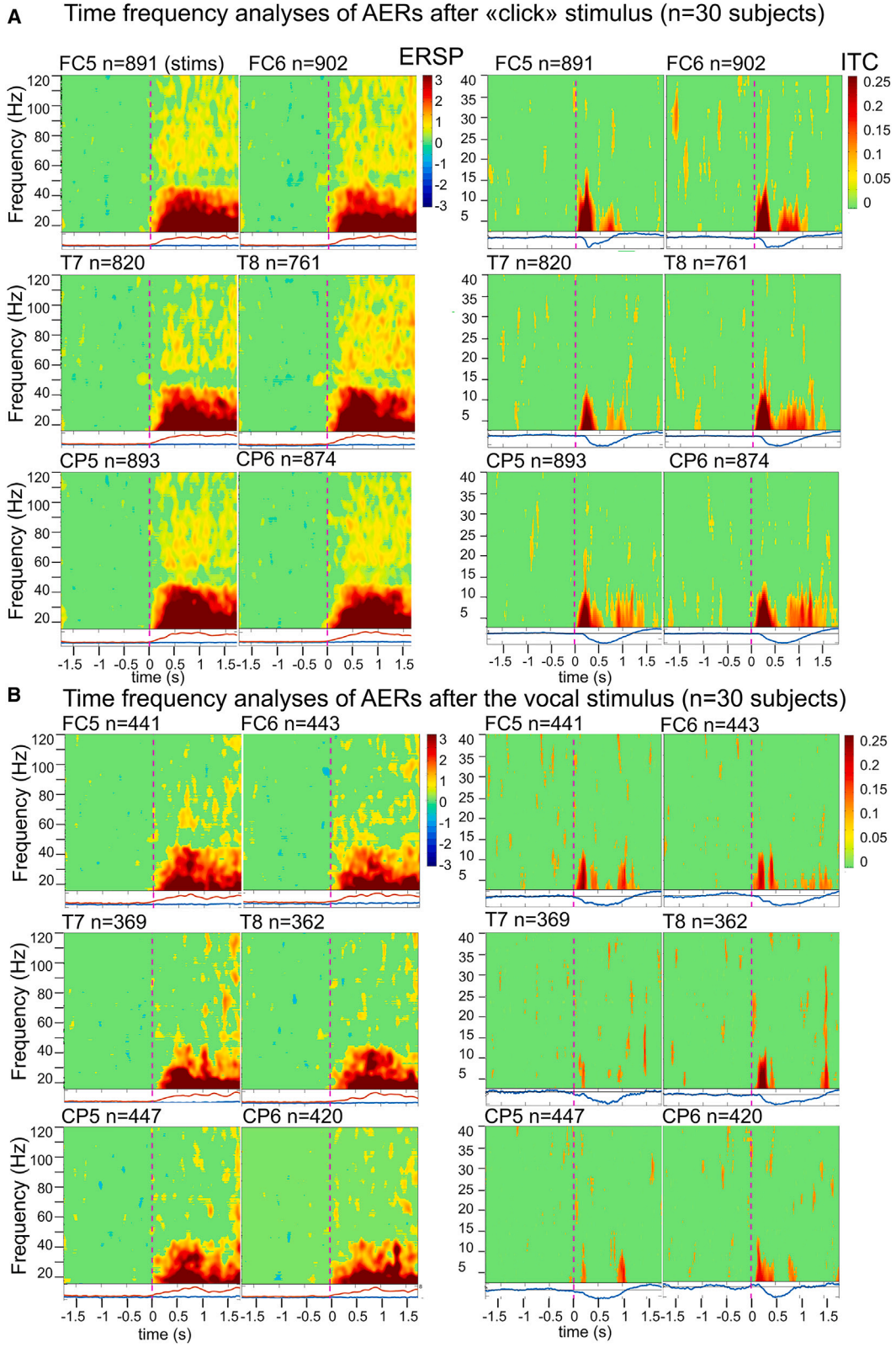

(legend on next page)

and topography of ERPs, as they lead to the activation of different tonotopic maps.[50] From birth, the generators of the main peak of auditory ERPs at term (P2) appear to have a well-defined tonotopic organization, and words evoke larger and more complex responses than tone bursts.[35] It is unclear whether sound intensity (70 dB SPL for "click" versus 50 dB SPL for voice) might play a role in our study, but the spectral content of the stimulus is more likely to account for the more spatially widespread and stronger spectral power increase after "click" since we previously reported that "click" at low intensity slightly exceeding the background noise level of the neonatal department was still able to evoke more prominent spectral power increase than the vocal stimulus at 70–75 dB SPL.[23] The stimulation protocol began with around 25 vocal, followed by "click" stimuli presented both every 10 s until awakening so, the fluctuation of vigilance (switch from the AS to QS) thus of responsiveness, might impact the results.[23,35] However, AS typically lasts 15–20 min between 32 and 36 PMW, so it was unlikely that the babies changed their sleep stage during the first 8 min (time needed for 50 stimuli).[51,52] Indeed, only 4 babies switched from AS to QS during the first 50 stimuli, others received both stimuli in AS (24) or in QS (2). To clarify this issue, we statistically compared the AERs at the beginning and the end of stimulus sequences and found no difference, which most likely eliminates a presentation order effect induced, for example, by a change in vigilance during the sequence. Habituation could also impact the AERs, however we used an inter-stimulus interval of 10 s for both stimuli which prevents habituation, since the fetal auditory memory window is about 800 ms and no short term habituation was observed in fetuses for inter-stimulus interval >2 s in auditory or visual modality.[53–57] The results of power spectrum analyses of AERs using 31 electrodes in the current study support our previous findings on EEG recordings with 9 electrodes and the same auditory stimuli administered randomly every 20 s during AS and QS sleep, showing that the vocal stimulus evokes AERs with weaker spectral power than "click".[23]

In the present study, AERs were studied only in sleep; however, sleep is the most representative behavioral state in fetuses which spend up to 90% of the time sleeping (around 60% in preterm babies hospitalized in ICU), and this also allows better quality of recordings.[52]

Studies of evoked EEG oscillations in infants showed that auditory ERPs result from the summation of oscillatory components in discrete bands (theta to gamma) which vary according to stimulus characteristics and are involved in auditory discrimination, rapid auditory processing, thus in language development.[58–60] Here we found in premature that AERs include oscillations in delta to beta bands with an inter-trial coherence (ITC) value up to 0.25, similar to that of ERPs evoked by pure tones and words in typically developing children at older ages.[42,61–63]

Here the phase synchronized oscillatory component occurred at the same time window as two well-known markers of cortical discriminative ability, fetal mismatch negativity (MMN, the waveform obtained by subtracting the evoked response to a standard sound from the response to a deviant one) and late discriminative negativity (LDN, the endogenous response). Using fetal MEG *in utero* between 32 and 35 PMW of age, the latency of response to a standard tone was 224 ± 43 ms, whereas MMN occurred at 318 ± 37 ms and LDN at 462 ± 33 ms.[53,64] Mento et al. (2010) observed late negative responses in temporal electrodes between 350 and 650 ms with higher amplitude on the right side, thus in favor of an early functional right lateralization of pitch processing (detection and discrimination) arising by 30 PMW.[38] MMN responses to phonetic and voice changes were also reported from 29 PMW.[34] The difference we presently found in the topography and the lateralization of evoked oscillations after two physically different auditory stimuli suggests that this oscillatory component underlies stimulus-specific processing within cortical networks as early as at the age equivalent of third trimester of gestation.

Preterm AERs include gamma oscillations with increasing power during the equivalent of the third trimester of gestation

We show here in preterm infants that AERs contain broad band oscillations including gamma in the frequency range of 30–40 Hz and that the power of these oscillations increased during the age equivalent of the third trimester of gestation. Using time-frequency and power spectrum analyses we also observed a high-gamma (>80 Hz) power increase after auditory stimuli but the true oscillatory nature of these changes could not be confirmed by visual analysis (as recommended for identification of the genuine gamma oscillations).[65] Evoked gamma oscillations have been observed in response to auditory, visual and somatosensory stimuli occurring ~100 ms after stimulus onset in humans.[66] This activity is relevant for the processing of specific sensory stimuli and its frequency varies depending on sensory modality, with auditory stimuli responding between 30 and 40 Hz and visual stimuli at higher frequencies within the gamma band.[66] Gamma oscillations up to 40 Hz were previously reported during spontaneous EEG activity and auditory evoked DBs in preterm, visual evoked responses in term neonates, and AERs in toddlers.[6,8,58,60,62,67,68] In infants, induced gamma oscillations have been detected in the anterior cingulate cortex during native language contrast discrimination, and since they can be modulated by active auditory experience, they were suggested to play a role in discrimination and language learning.[59,60]

As suggested by the intracortical and thalamic recordings of sensory evoked oscillations in the neonatal rat model, the early

Figure 8. Event-related spectral perturbations (ERSP) (in the 10 to 120 Hz frequency band) after "click" and voice (left) and corresponding inter-trial coherence (ITC) analysis (in 3–40 Hz) (right) (n = 30 subjects)

ERSP in 30 subjects aged 30 to 38 PMW using all available "click" (A) and voice (B) artifact free epochs with stimuli (n). Colors represent t-statistics after application of a significance threshold mask ($p < 0.05$ corrected for multiple comparisons across time, frequency and channel dimensions, using the false discovery rate method). Significant ERSP, corresponding to an increase in oscillation amplitude compared to the pre-stimulus baseline at frequencies from alpha to high-gamma bands at all targeted FC5-6, T7-8, and CP5-6 electrodes are shown ($p < 0.05$, FDR-corrected for multiple comparisons across time, frequency and sensors).

Visual and spectral power density analyses (32 PMW preterm)

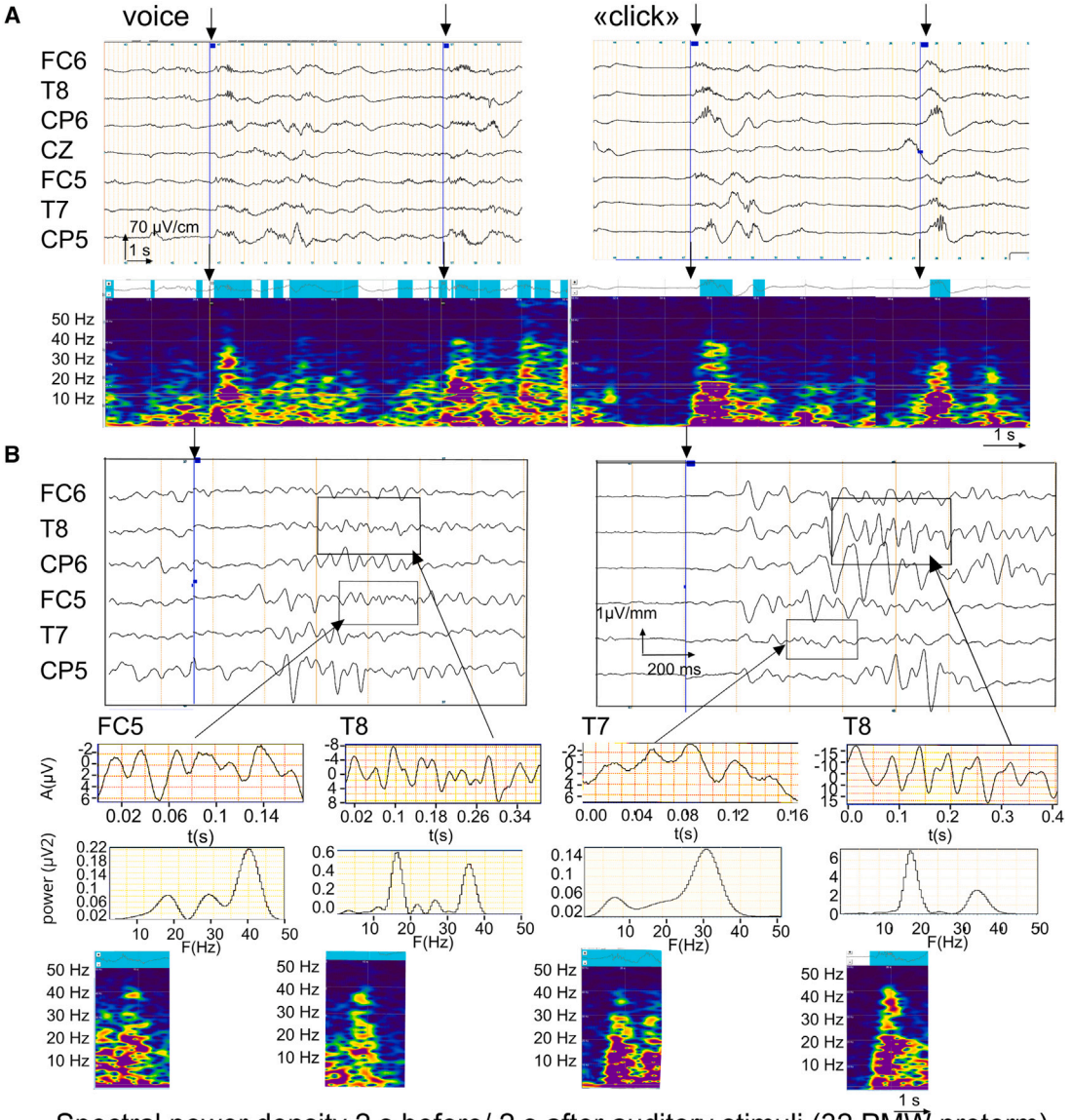

Spectral power density 2 s before/ 2 s after auditory stimuli (32 PMW preterm)

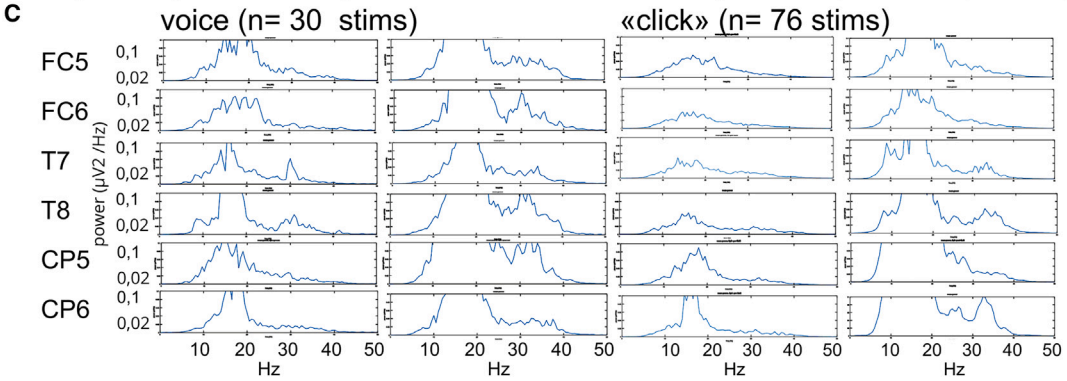

(legend on next page)

component of AERs in preterm infants likely involves thalamic bursts organized in fast oscillations (including gamma rhythmic activity)[14,15] as well as intra-cortical processing in the primary auditory cortex and cortico-thalamic feedback (generating larger scale patterning at alpha-beta frequencies).[15,25,69–72] Gamma oscillations as part of the sensory evoked response were widely studied by invasive procedures in animals and scalp-recorded potentials in human adults.[73–78] It has been shown in primates that stimulus characteristics such as contrast modulate gamma oscillations in the 30–80 Hz band in the visual evoked response in V1 cortex.[78] Gamma oscillations are essential for the precise timing of neuronal-spike discharges, thus information encoding, transmission and perception, and are deficient in neurodevelopmental disorders such as schizophrenia and autism spectrum disorders in adults and children.[63,79–84]

In the neocortex, gamma oscillations during sensory processing result in the co-activation of reciprocally connected groups of pyramidal neurons and interneurons.[79,81] Stimulus evoked gamma oscillations are primarily generated in layer 4 and supragranular layers and entrain pyramidal excitatory neurons and GABAergic interneurons, including fast-spiking parvalbumin basket cells,[81,85] involving both feedforward synchronization by gamma-rhythmic thalamic inputs and intracortical, largely inhibition based gamma synchronization.[86–89] In neonatal rodents, sensory-evoked early gamma oscillations are generated primarily via feedforward thalamic gamma-excitation with limited participation of cortical interneurons during the first 2–3 postnatal days (P).[14,15] Starting from P4-5, GABAergic interneurons begin to participate in the patterning of gamma oscillations and the suppression of the horizontal spread of alpha-beta oscillations of the spindle-bursts along with the formation of recurrent excitatory and inhibitory synaptic circuits.[14,70,90–92] Our results showing the increase of auditory evoked gamma power during the equivalent of the third trimester of gestational age in humans are also consistent with a maturation of excitatory and inhibitory cortical circuits during this synaptic "spurt" period.[1,93–95] Indeed, the important period for GABAergic network development in the human cerebral cortex, with increasing of GABAergic receptors and of interneuron density, occurs during the late third trimester of pregnancy also with a peak at term.[96–98] Interestingly, spontaneous and evoked DBs begin to decrease from around 35 PMW when the GABAergic neuronal density increases.[8,23,99,100] The increasing GABAergic inhibition seems therefore to shape the cortical sensory-evoked responses to more spatially and temporally restricted responses.[101] Increasing gamma oscillations likely mark the development of cortical inhibition required for the precise timing of sensory processing and information encoding.[14,80,101,102]

Interspecies comparisons

Current knowledge on the developmental physiology of the auditory system is largely based on results obtained in altricious animal models, notably rodents. With their ear canal closed, rats are born deaf (prehearing); they start hearing high intensity sounds through bone-conduction from P8 (high-threshold hearing) and normal intensity sounds from P13 (low-threshold hearing).[7,25] The onset of low-threshold hearing is a crucial developmental milestone as it heralds the opening of the critical period of activity-dependent plasticity in the auditory cortex lasting for about three days and resulting in the refinement of the tonotopic maps.[103] A similar sequence can be observed in other rodents (mouse, gerbil) and in ferrets.[22,104,105] It is of note that the crude tonotopic organization of the auditory cortex emerges before hearing onset, as evidenced by the topography of the responses evoked by inferior colliculus stimulation.[25] This is also evidenced by mesoscale calcium imaging studies which showed that the regions in the inferior colliculus and auditory cortex encoding similar sound frequencies exhibit synchronous bursts of spontaneous cochlea – driven activity that stops just at the onset of low-threshold hearing along with the cessation of spontaneous bursting of spiral ganglion neurons and ATP release from inner supporting cells.[10,12,106,107] Spontaneous cochlear activity, which is likely at the origin of spontaneous otoacoustic emissions in humans, also likely drives spontaneous DBs in the auditory cortex of preterm neonates. The early tonotopic organization of the auditory cortex also likely accounts for the stimulus-specific topography of AER that we found in the present study. Moreover, sensory responses in rats during the low-threshold hearing period are characterized by intracolumnar activity propagation and intracortical horizontal activity spread from the primary auditory cortex toward higher level processing cortical regions,[25] which is consistent with the propagation profiles of the AERs we have observed in preterm neonates.

Together, these interspecies comparisons suggest that the fundamental principles of developing auditory system are conserved across mammalian evolution, with both spontaneous (cochlear-driven) and sensory signals cooperating in driving activity in the auditory cortex during the corresponding developmental stages of the second postnatal week in rodents and the third trimester of gestation in humans. Similar principles may

Figure 9. Visual and power spectrum density analyses of gamma oscillations

Example of EEG recording (A) with average reference in a 32 PMW preterm showing AERs including delta brushes (DBs) evoked by the auditory stimuli, voice and "click" on the FC5, FC6, T7, T8, CP5, and CP6 electrodes with corresponding wavelet analysis (high pass filter: 0.53 Hz, low pass filter: 120 Hz; notch filter: 50 Hz, upward deflection represents negative potential. Visual identification of gamma oscillations (framed) on the main electrodes involved in AERs (FC5, FC6, T7, T8, CP5, and CP6).

(B) EEG is represented after maximal amplification (1 μV/mm) on 1, 5 s timescale with 15.9 Hz and 120 Hz high and low pass filter respectively. Power spectrum density and wavelet analyses of gamma oscillations are represented below (EEG review software Natus-Coherence).

(C) Mean power spectrum density analysis of AERs (2 s before and after vocal and "click" stimuli) showed a broad band (delta to gamma) increase of oscillations with for gamma a narrow peak between 30 and 40 Hz on the FC6, T8, and CP5 electrodes for voice and the T8 and CP6 electrodes for "click" (GNU Octave software).

also operate across mammals in other sensory systems, such as the somatosensory and visual modalities.[2,6,95,108,109]

Conclusion

Together, these results in preterm human newborns show that during the third trimester of gestation, physically different auditory stimuli evoke AERs (including their late DB component) which display different spatiotemporal dynamics and oscillatory activity profiles with different developmental trajectories. This capacity to process physically different auditory signals into specific cortical networks suggests that the auditory system already achieves a remarkable level of maturity within the preterm period and probably supports some early emerging cognitive abilities in the human fetus. We also hypothesize that the DBs, which exhibit stimulus-specific propagation profiles, are involved in the early formation of high-order auditory cortical networks.

Limitations of the study

While the present study was initially designed to unravel the neurophysiological basis for the ability to recognize a human voice by the preterm infant, and although the results are in keeping with this ability to discriminate verbal and non-verbal auditory stimuli, several limitations must be taken into account. The first is that the two stimuli were not normalized for intensity, duration, or acoustic frequency spectrum so that we were not able to conclude if the difference of the AERs arises from the verbal component or from other physical characteristics of these stimuli. In addition, while we presented an anonymous human voice to the babies, in future studies it would also be of interest to investigate whether and how preterm babies are able to discriminate and differently process the voices of mother and father and third persons. Our comparative analysis of individual ERP's latencies and amplitudes after both stimuli and its evolution with gestational age was underpowered since it concerned only 9 subjects. Moreover, our protocol design used non-randomly presented stimuli, so that the fluctuation of vigilance (switch from the AS to QS), thus of responsiveness, and the habituation effect might impact the results. The influence of sex on AERs after both stimuli was not analyzed in our population; however if any, the impact on group-level studies was similar since the sex ratio was of 1:14. There is a legal and ethical prohibition to record the ethnical race in French law; the data on race and ethnicity were therefore not registered in our study. Power spectrum and time frequency analyses showed increased broadband high-gamma (>80 Hz) power, however, these findings on high-gamma were not confirmed by visual analysis of the time-series data. This could be explained by the low signal-to-noise ratio (SNR) due to many artifacts from the machinery in the ICU environment, physiological artifacts from EMG (facial movements), and the large powerline and its harmonic artifacts. Increased broadband high-gamma power could also be misinterpreted since non-oscillatory features may contribute to the power spectral density, such as increased neuronal firing during DBs in the absence of any genuine high-gamma oscillations or resulting from other non-oscillatory components such as sharp transients (voltage deflections with steep gradients).[65] Further study using better technical conditions at the time of EEG acquisition, notably reduced powerline noise with appropriate electric shielding and better SNR, should delineate the frequency spectrum of AERs in the gamma band with better precision. Improved signal analyses removing EOG and EMG artifacts through ICA procedures should also improve the delineation of high-gamma oscillations in the premature infant.

RESOURCE AVAILABILITY

Lead contact

Further information and requests for resources should be directed to and will be fulfilled by the Lead Contact: Anna Kaminska, MD, Ph-D; E-mail; (anna.kaminska@aphp.fr).

Materials availability

Written informed consent was obtained from all parents. The procedure was in accordance with the Ethics Code of the World Medical Association, was approved by our institutional review board, INSERM (French National Institute of Medical Research) Ethics Committee (N° 2751), and was registered as a Clinical Research Study "Early EEG activities in preterm infant" (N° ID-RCB:2008-A0147-49), (French Research Agency https://anr.fr/Projet-ANR-09-MNPS-0006).

Data and code availability

Data

EEG epochs including auditory stimuli, generated in this study as well as frequency power spectrum (PS) values of mean-referenced signals computed over 2-s time intervals before and after the stimulus using the Fast Fourier Transform are available on request from the lead contact: Anna Kaminska MD, Ph-D (anna.kaminska@aphp.fr) on https://doi.org/10.57745/XPXYHR (https://entrepot.recherche.data.gouv.fr/dataset.xhtml?persistentId=doi:10.57745/XPXYHR).

Code

All original code has been deposited on Mendeley data (https://data.mendeley.com/) and is publicly available at https://doi.org/10.17632/7S382FS2BG.2 under name Auditory evoked delta brushes involve stimulus-specific cortical networks in preterm infants. MATLAB codes used for ERP analysis (Figures 3, 7 and S2) are pooled in "Analysis code for publication" folder of the Mendeley data repository with the following names: Fig3_A_BasicProtocols.m (database generation), Fig3A_B_CAEP_0.m (computation of average evoked potentials) Fig3C_C1_BBvsCLIC.m (comparison of evoked potentials between vocal and click stimuli) FigS2_C1b_BBvsCLIC_FirstVsLastStim.m (comparison of evoked potentials between first and last stimuli) Fig7_C2_BBvsCLIC_TF.m (comparison of time-frequency maps between vocal and click stimuli) Fig3_process_nt_smooth.m (EEG data preprocessing). MATLAB code used for Figure S3 is available under name S3.m.

Other items

This study was a part of a clinical trial registered as a Clinical Research Study "Early EEG activities in preterm infant" (N° ID-RCB: 2008-A0147-49), French Research Agency https://anr.fr/Projet-ANR-09-MNPS-0006).

ACKNOWLEDGMENTS

This work was supported by the French Agency for Research (https://anr.fr/Projet-ANR-09-MNPS-0006) and the Fondation de France (https://www.fondationdefrance.org/fr) (FDF-2017-00079262) J.D. was supported by the Médisite Foundation (FDF-2018-00092867) and the IdEx Université de Paris (ANR-18-IDEX-0001).

We thank Pr Petra Hüppi (from Geneva University Hospitals) for providing the preterm MRI data. We thank Daniele Decarpentry and Maurice Lemeux for recordings in infants, Mike Sintsov for help with analysis, as well as Walter Janssens and Laurent Fousseret (Natus France) for technical assistance and software adaptation for the purpose of this research project. We thank Pascal Benquet and Amar Kachenoura (University of Rennes, INSERM U 1099, LTSI) for help with the analyses of neural oscillations.

AUTHOR CONTRIBUTIONS

Conceptualization, A.K., D.A., V.D., C.C., M.K., J.D., and R.K.; methodology, A.K., D.A., V.D., F.W., Y.D., J.D., and R.K.; investigation, A.K., J.-F.M., S.H., M.M., C.C., and R.K.; Resources, A.K., D.A., V.D., J.-F.M., S.H., A.M., A.B., L.O.-R., M.K., and J.D.; data curation, A.K., D.A., V.D., A.M., Y.D., and M. K.; validation, A.K., D.A., V.D., F.W., Y.D., M.K., C.C., J.D., and R.K.; formal analysis, D.A., V.D., J.L., A.M., A.B., Y.D., M.K., J.D., and R.K.; writing – original draft, A.K., D.A., V.D., J.L., C.C., M.K., J.D., and R.K.; writing – review and editing, A.K., D.A., V.D., J.L., J.-F.M., S.H., M.M., A.M., A.B., L.H.-P., C.C., F.W., Y.D., M.K., J.D., and R.K; visualization, A.K., D.A., V.D., J.L., Y.D., M.K., and J.D.; funding acquisition, A.K., C.C., J.D., and R.K.; supervision, A.K., D.A., C.C., Y.D., J.D., and R.K.; project administration, A.K., L.H.-P., C.C., J.D., and R.K.

DECLARATION OF INTERESTS

The authors declare no competing interests.

STAR★METHODS

Detailed methods are provided in the online version of this paper and include the following:

- KEY RESOURCES TABLE
- **EXPERIMENTAL MODEL AND STUDY PARTICIPANT DETAILS**
  - *Subjects and EEG recording protocol*
  - Subjects
  - EEG recording
  - Auditory stimuli
  - Vigilance stage
- **METHOD DETAILS**
  - *Visual inspection of EEG*
  - *Auditory event related potentials analyses (ERPs)*
  - *Frequency power spectrum (PS) analyses*
  - *Time–frequency analyses*
- **QUANTIFICATION AND STATISTICAL ANALYSES**

SUPPLEMENTAL INFORMATION

Supplemental information can be found online at https://doi.org/10.1016/j.isci.2025.112313.

Received: June 10, 2023
Revised: October 16, 2023
Accepted: March 25, 2025
Published: March 27, 2025

REFERENCES

1. Clancy, B., Darlington, R.B., and Finlay, B.L. (2001). Translating developmental time across mammalian species. Neuroscience *105*, 7–17. https://doi.org/10.1016/s0306-4522(01)00171-3.
2. Hanganu-Opatz, I.L. (2010). Between molecules and experience: role of early patterns of coordinated activity for the development of cortical maps and sensory abilities. Brain Res. Rev. *64*, 160–176. https://doi.org/10.1016/j.brainresrev.2010.03.005.
3. Khazipov, R., and Luhmann, H.J. (2006). Early patterns of electrical activity in the developing cerebral cortex of humans and rodents. Trends Neurosci. *29*, 414–418. https://doi.org/10.1016/j.tins.2006.05.007.
4. Luhmann, H.J., Sinning, A., Yang, J.W., Reyes-Puerta, V., Stüttgen, M.C., Kirischuk, S., and Kilb, W. (2016). Spontaneous Neuronal Activity in Developing Neocortical Networks: From Single Cells to Large-Scale Interactions. Front. Neural Circuits *10*, 40. https://doi.org/10.3389/fncir.2016.00040.
5. Luhmann, H.J., Kanold, P.O., Molnár, Z., and Vanhatalo, S. (2022). Early brain activity: Translations between bedside and laboratory. Prog. Neurobiol. *213*, 102268. https://doi.org/10.1016/j.pneurobio.2022.102268.
6. Milh, M., Kaminska, A., Huon, C., Lapillonne, A., Ben-Ari, Y., and Khazipov, R. (2007). R apid cortical oscillations and early motor activity in premature human neonate. Cereb. Cortex *17*, 1582–1594. https://doi.org/10.1093/cercor/bhl069.
7. Colonnese, M.T., Kaminska, A., Minlebaev, M., Milh, M., Bloem, B., Lescure, S., Moriette, G., Chiron, C., Ben-Ari, Y., and Khazipov, R. (2010). A conserved switch in sensory processing prepares developing neocortex for vision. Neuron *67*, 480–498. https://doi.org/10.1016/j.neuron.2010.07.015.
8. Kaminska, A., Delattre, V., Laschet, J., Dubois, J., Labidurie, M., Duval, A., Manresa, A., Magny, J.F., Hovhannisyan, S., Mokhtari, M., et al. (2018). Cortical Auditory-Evoked Responses in Preterm Neonates: Revisited by Spectral and Temporal Analyses. Cereb. Cortex *28*, 3429–3444. https://doi.org/10.1093/cercor/bhx206.
9. Lippe, W.R. (1994). Rhythmic spontaneous activity in the developing avian auditory system. J. Neurosci. *14*, 1486–1495. https://doi.org/10.1523/JNEUROSCI.14-03-01486.1994.
10. Tritsch, N.X., and Bergles, D.E. (2010). Developmental regulation of spontaneous activity in the Mammalian cochlea. J. Neurosci. *30*, 1539–1550. https://doi.org/10.1523/JNEUROSCI.3875-09.2010.
11. Blankenship, A.G., and Feller, M.B. (2010). Mechanisms underlying spontaneous patterned activity in developing neural circuits. Nat. Rev. Neurosci. *11*, 18–29. https://doi.org/10.1038/nrn2759.
12. Babola, T.A., Li, S., Gribizis, A., Lee, B.J., Issa, J.B., Wang, H.C., Crair, M.C., and Bergles, D.E. (2018). Homeostatic Control of Spontaneous Activity in the Developing Auditory System. Neuron *99*, 511–524.e5. https://doi.org/10.1016/j.neuron.2018.07.004.
13. Wang, H.C., and Bergles, D.E. (2015). Spontaneous activity in the developing auditory system. Cell Tissue Res. *361*, 65–75. https://doi.org/10.1007/s00441-014-2007-5.
14. Minlebaev, M., Colonnese, M., Tsintsadze, T., Sirota, A., and Khazipov, R. (2011). Early γ oscillations synchronize developing thalamus and cortex. Science (New York, N.Y.) *334*, 226–229. https://doi.org/10.1126/science.1210574.
15. Yang, J.W., An, S., Sun, J.J., Reyes-Puerta, V., Kindler, J., Berger, T., Kilb, W., and Luhmann, H.J. (2013). Thalamic network oscillations synchronize ontogenetic columns in the newborn rat barrel cortex. Cereb. Cortex *23*, 1299–1316. https://doi.org/10.1093/cercor/bhs103.
16. An, S., Kilb, W., and Luhmann, H.J. (2014). Sensory-evoked and spontaneous gamma and spindle bursts in neonatal rat motor cortex. J. Neurosci. *34*, 10870–10883. https://doi.org/10.1523/JNEUROSCI.4539-13.2014.
17. Luhmann, H.J., and Khazipov, R. (2018). Neuronal activity patterns in the developing barrel cortex. Neuroscience *368*, 256–267. https://doi.org/10.1016/j.neuroscience.2017.05.025.
18. Molnár, Z., Luhmann, H.J., and Kanold, P.O. (2020). Transient cortical circuits match spontaneous and sensory-driven activity during development. Science (New York, N.Y.) *370*, eabb2153. https://doi.org/10.1126/science.abb2153.
19. Chang, M., and Kanold, P.O. (2021). Development of Auditory Cortex Circuits. J. Assoc. Res. Otolaryngol. *22*, 237–259. https://doi.org/10.1007/s10162-021-00794-3.
20. Martini, F.J., Guillamón-Vivancos, T., Moreno-Juan, V., Valdeolmillos, M., and López-Bendito, G. (2021). Spontaneous activity in developing thalamic and cortical sensory networks. Neuron *109*, 2519–2534. https://doi.org/10.1016/j.neuron.2021.06.026.
21. Antón-Bolaños, N., Sempere-Ferràndez, A., Guillamón-Vivancos, T., Martini, F.J., Pérez-Saiz, L., Gezelius, H., Filipchuk, A., Valdeolmillos, M., and López-Bendito, G. (2019). Prenatal activity from thalamic neurons governs the emergence of functional cortical maps in mice.

Science (New York, N.Y.) *364*, 987–990. https://doi.org/10.1126/science.aav7617.

22. Meng, X., Mukherjee, D., Kao, J.P.Y., and Kanold, P.O. (2021). Early peripheral activity alters nascent subplate circuits in the auditory cortex. Sci. Adv. *7*, eabc9155. https://doi.org/10.1126/sciadv.abc9155.
23. Chipaux, M., Colonnese, M.T., Mauguen, A., Fellous, L., Mokhtari, M., Lezcano, O., Milh, M., Dulac, O., Chiron, C., Khazipov, R., and Kaminska, A. (2013). Auditory stimuli mimicking ambient sounds drive temporal "delta-brushes" in premature infants. PLoS One *8*, e79028. https://doi.org/10.1371/journal.pone.0079028.
24. Fabrizi, L., Worley, A., Patten, D., Holdridge, S., Cornelissen, L., Meek, J., Boyd, S., and Slater, R. (2011). Electrophysiological measurements and analysis of nociception in human infants. J. Vis. Exp. *20*, pii3118.
25. Makarov, R., Sintsov, M., Valeeva, G., Starikov, P., Negrov, D., and Khazipov, R. (2021). Bone conducted responses in the neonatal rat auditory cortex. Sci. Rep. *11*, 16777. https://doi.org/10.1038/s41598-021-96188-9.
26. Stjerna, S., Voipio, J., Metsäranta, M., Kaila, K., and Vanhatalo, S. (2012). Preterm EEG: a multimodal neurophysiological protocol. J. Vis. Exp., 3774. https://doi.org/10.3791/3774.
27. Colonnese, M.T., and Phillips, M.A. (2018). Thalamocortical function in developing sensory circuits. Curr. Opin. Neurobiol. *52*, 72–79. https://doi.org/10.1016/j.conb.2018.04.019.
28. Turkewitz, G., Birch, H.G., and Cooper, K.K. (1972). Responsiveness to simple and complex auditory stimuli in the human newborn. Dev. Psychobiol. *5*, 7–19. https://doi.org/10.1002/dev.420050103.
29. DeCasper, A.J., and Fifer, W.P. (1980). Of human bonding: newborns prefer their mothers' voices. Science (New York, N.Y.) *208*, 1174–1176. https://doi.org/10.1126/science.7375928.
30. Shahidullah, S., and Hepper, P.G. (1994). Frequency discrimination by the fetus. Early Hum. Dev. *36*, 13–26. https://doi.org/10.1016/0378-3782(94)90029-9.
31. Lecanuet, J.P., Graniere-Deferre, C., Jacquet, A.Y., and DeCasper, A.J. (2000). Fetal discrimination of low-pitched musical notes. Dev. Psychobiol. *36*, 29–39.
32. Granier-Deferre, C., Bassereau, S., Ribeiro, A., Jacquet, A.Y., and Decasper, A.J. (2011). A melodic contour repeatedly experienced by human near-term fetuses elicits a profound cardiac reaction one month after birth. PLoS One *6*, e17304. https://doi.org/10.1371/journal.pone.0017304.
33. Mahmoudzadeh, M., Dehaene-Lambertz, G., Fournier, M., Kongolo, G., Goudjil, S., Dubois, J., Grebe, R., and Wallois, F. (2013). Syllabic discrimination in premature human infants prior to complete formation of cortical layers. Proc. Natl. Acad. Sci. USA *110*, 4846–4851. https://doi.org/10.1073/pnas.1212220110.
34. Mahmoudzadeh, M., Wallois, F., Kongolo, G., Goudjil, S., and Dehaene-Lambertz, G. (2017). Functional Maps at the Onset of Auditory Inputs in Very Early Preterm Human Neonates. Cereb. Cortex *27*, 2500–2512. https://doi.org/10.1093/cercor/bhw103.
35. Wunderlich, J.L., and Cone-Wesson, B.K. (2006). Maturation of CAEP in infants and children: a review. Hear. Res. *212*, 212–223. https://doi.org/10.1016/j.heares.2005.11.008.
36. Näätänen, R., and Picton, T. (1987). The N1 wave of the human electric and magnetic response to sound: a review and an analysis of the component structure. Psychophysiology *24*, 375–425. https://doi.org/10.1111/j.1469-8986.1987.tb00311.x.
37. Shahin, A.J., Roberts, L.E., Miller, L.M., McDonald, K.L., and Alain, C. (2007). Sensitivity of EEG and MEG to the N1 and P2 auditory evoked responses modulated by spectral complexity of sounds. Brain Topogr. *20*, 55–61. https://doi.org/10.1007/s10548-007-0031-4.
38. Mento, G., Suppiej, A., Altoè, G., and Bisiacchi, P.S. (2010). Functional hemispheric asymmetries in humans: electrophysiological evidence from preterm infants. Eur. J. Neurosci. *31*, 565–574. https://doi.org/10.1111/j.1460-9568.2010.07076.x.
39. Rotteveel, J.J., de Graaf, R., Stegeman, D.F., Colon, E.J., and Visco, Y.M. (1987). The maturation of the central auditory conduction in preterm infants until three months post term. V. The auditory cortical response (ACR). Hear. Res. *27*, 95–110. https://doi.org/10.1016/0378-5955(87)90029-3.
40. Hrbek, A., Karlberg, P., and Olsson, T. (1973). Development of visual and somatosensory evoked responses in pre-term newborn infants. Electroencephalogr. Clin. Neurophysiol. *34*, 225–232. https://doi.org/10.1016/0013-4694(73)90249-6.
41. Mento, G., and Bisiacchi, P.S. (2012). Neurocognitive development in preterm infants: insights from different approaches. Neurosci. Biobehav. Rev. *36*, 536–555. https://doi.org/10.1016/j.neubiorev.2011.08.008.
42. Yu, L., Wang, S., Huang, D., Wu, X., and Zhang, Y. (2018). Role of inter-trial phase coherence in atypical auditory evoked potentials to speech and nonspeech stimuli in children with autism. Clin. Neurophysiol. *129*, 1374–1382. https://doi.org/10.1016/j.clinph.2018.04.599.
43. Cheour-Luhtanen, M., Alho, K., Sainio, K., Rinne, T., Reinikainen, K., Pohjavuori, M., Renlund, M., Aaltonen, O., Eerola, O., and Näätänen, R. (1996). The ontogenetically earliest discriminative response of the human brain. Psychophysiology *33*, 478–481. https://doi.org/10.1111/j.1469-8986.1996.tb01074.x.
44. Schleussner, E., Schneider, U., Arnscheidt, C., Kähler, C., Haueisen, J., and Seewald, H.J. (2004). Prenatal evidence of left-right asymmetries in auditory evoked responses using fetal magnetoencephalography. Early Hum. Dev. *78*, 133–136. https://doi.org/10.1016/j.earlhumdev.2004.03.005.
45. Dehaene-Lambertz, G., Dehaene, S., and Hertz-Pannier, L. (2002). Functional neuroimaging of speech perception in infants. Science (New York, N.Y.) *298*, 2013–2015. https://doi.org/10.1126/science.1077066.
46. Ghio, M., Cara, C., and Tettamanti, M. (2021). The prenatal brain readiness for speech processing: A review on foetal development of auditory and primordial language networks. Neurosci. Biobehav. Rev. *128*, 709–719. https://doi.org/10.1016/j.neubiorev.2021.07.009.
47. Thomason, M.E., Grove, L.E., Lozon, T.A., Jr., Vila, A.M., Ye, Y., Nye, M.J., Manning, J.H., Pappas, A., Hernandez-Andrade, E., Yeo, L., et al. (2015). Age-related increases in long-range connectivity in fetal functional neural connectivity networks in utero. Dev. Cogn. Neurosci. *11*, 96–104.
48. Vannest, J.J., Karunanayaka, P.R., Altaye, M., Schmithorst, V.J., Plante, E.M., Eaton, K.J., Rasmussen, J.M., and Holland, S.K. (2009). Comparison of fMRI data from passive listening and active-response story processing tasks in children. J. Magn. Reson. Imaging. *29*, 971–976. https://doi.org/10.1002/jmri.21694.
49. Vouloumanos, A., Kiehl, K.A., Werker, J.F., and Liddle, P.F. (2001). Detection of sounds in the auditory stream: event-related fMRI evidence for differential activation to speech and nonspeech. J. Cogn. Neurosci. *13*, 994–1005. https://doi.org/10.1162/089892901753165890.
50. Saenz, M., and Langers, D.R.M. (2014). Tonotopic mapping of human auditory cortex. Hear. Res. *307*, 42–52. https://doi.org/10.1016/j.heares.2013.07.016.
51. Curzi-Dascalova, L., Figueroa, J.M., Eiselt, M., Christova, E., Virassamy, A., d'Allest, A.M., Guimarâes, H., Gaultier, C., and Dehan, M. (1993). Sleep state organization in premature infants of less than 35 weeks' gestational age. Pediatr. Res. *34*, 624–628. https://doi.org/10.1203/00006450-199311000-00013.
52. Ryan, M.A.J., Mathieson, S.R., Livingstone, V., O'Sullivan, M.P., Dempsey, E.M., and Boylan, G.B. (2023). Sleep state organisation of moderate to late preterm infants in the neonatal unit. Pediatr. Res. *93*, 595–603. https://doi.org/10.1038/s41390-022-02319-x.
53. Draganova, R., Eswaran, H., Murphy, P., Huotilainen, M., Lowery, C., and Preissl, H. (2005). Sound frequency change detection in fetuses and

newborns, a magnetoencephalographic study. Neuroimage *28*, 354–361. https://doi.org/10.1016/j.neuroimage.2005.06.011.

54. Cheour, M., Ceponiené, R., Leppänen, P., Alho, K., Kujala, T., Renlund, M., Fellman, V., and Näätänen, R. (2002). The auditory sensory memory trace decays rapidly in newborns. Scand. J. Psychol. *43*, 33–39. https://doi.org/10.1111/1467-9450.00266.
55. Muenssinger, J., Matuz, T., Schleger, F., Kiefer-Schmidt, I., Goelz, R., Wacker-Gussmann, A., Birbaumer, N., and Preissl, H. (2013 a). Auditory habituation in the fetus and neonate: an fMEG study. Dev. Sci. *16*, 287–295. https://doi.org/10.1111/desc.12025.
56. Muenssinger, J., Stingl, K.T., Matuz, T., Binder, G., Ehehalt, S., and Preissl, H. (2013 b). Auditory habituation to simple tones: reduced evidence for habituation in children compared to adults. Front. Hum. Neurosci. *7*, 377. https://doi.org/10.3389/fnhum.2013.00377.
57. Sheridan, C.J., Preissl, H., Siegel, E.R., Murphy, P., Ware, M., Lowery, C.L., and Eswaran, H. (2008). Neonatal and fetal response decrement of evoked responses: a MEG study. Clin. Neurophysiol. *119*, 796–804. https://doi.org/10.1016/j.clinph.2007.11.174.
58. Musacchia, G., Ortiz-Mantilla, S., Realpe-Bonilla, T., Roesler, C.P., and Benasich, A.A. (2015). Infant Auditory Processing and Event-related Brain Oscillations. J. Vis. Exp. e52420. https://doi.org/10.3791/52420.
59. Musacchia, G., Ortiz-Mantilla, S., Choudhury, N., Realpe-Bonilla, T., Roesler, C., and Benasich, A.A. (2017). Active auditory experience in infancy promotes brain plasticity in Theta and Gamma oscillations. Dev. Cogn. Neurosci. *26*, 9–19. https://doi.org/10.1016/j.dcn.2017.04.004.
60. Ortiz-Mantilla, S., Hämäläinen, J.A., Musacchia, G., and Benasich, A.A. (2013). Enhancement of gamma oscillations indicates preferential processing of native over foreign phonemic contrasts in infants. J. Neurosci. *33*, 18746–18754. https://doi.org/10.1523/JNEUROSCI.3260-13.2013.
61. Gilley, P.M., Sharma, M., and Purdy, S.C. (2016). Oscillatory decoupling differentiates auditory encoding deficits in children with listening problems. Clin. Neurophysiol. *127*, 1618–1628. https://doi.org/10.1016/j.clinph.2015.11.003.
62. Cantiani, C., Ortiz-Mantilla, S., Riva, V., Piazza, C., Bettoni, R., Musacchia, G., Molteni, M., Marino, C., and Benasich, A.A. (2019). Reduced left-lateralized pattern of event-related EEG oscillations in infants at familial risk for language and learning impairment. Neuroimage. Clin. *22*, 101778. https://doi.org/10.1016/j.nicl.2019.101778.
63. Ortiz-Mantilla, S., Cantiani, C., Shafer, V.L., and Benasich, A.A. (2019). Minimally-verbal children with autism show deficits in theta and gamma oscillations during processing of semantically-related visual information. Sci. Rep. *9*, 5072. https://doi.org/10.1038/s41598-019-41511-8.
64. Draganova, R., Eswaran, H., Murphy, P., Lowery, C., and Preissl, H. (2007). Serial magnetoencephalographic study of fetal and newborn auditory discriminative evoked responses. Early Hum. Dev. *83*, 199–207. https://doi.org/10.1016/j.earlhumdev.2006.05.018.
65. Hudson, M.R., and Jones, N.C. (2022). Deciphering the code: Identifying true gamma neural oscillations. Exp. Neurol. *357*, 114205. https://doi.org/10.1016/j.expneurol.2022.114205.
66. Pantev, C. (1995). Evoked and induced gamma-band activity of the human cortex. Brain Topogr. *7*, 321–330. https://doi.org/10.1007/BF01195258.
67. Grieve, P.G., Isler, J.R., Izraelit, A., Peterson, B.S., Fifer, W.P., Myers, M.M., and Stark, R.I. (2008). EEG functional connectivity in term age extremely low birth weight infants. Clin. Neurophysiol. *119*, 2712–2720. https://doi.org/10.1016/j.clinph.2008.09.020.
68. Isler, J.R., Grose-Fifer, J., Fifer, W.P., Housman, S., Stark, R.I., and Grieve, P.G. (2007). Frequency domain analyses of neonatal flash VEP. Pediatr. Res. *62*, 581–585. https://doi.org/10.1203/PDR.0b013e31815586a1.
69. Contreras, D., Destexhe, A., Sejnowski, T.J., and Steriade, M. (1996). Control of spatiotemporal coherence of a thalamic oscillation by cortico-thalamic feedback. Science (New York, N.Y.) *274*, 771–774. https://doi.org/10.1126/science.274.5288.771.
70. Minlebaev, M., Ben-Ari, Y., and Khazipov, R. (2007). Network mechanisms of spindle-burst oscillations in the neonatal rat barrel cortex in vivo. J. Neurophysiol. *97*, 692–700. https://doi.org/10.1152/jn.00759.2006.
71. Yang, J.W., Hanganu-Opatz, I.L., Sun, J.J., and Luhmann, H.J. (2009). Three patterns of oscillatory activity differentially synchronize developing neocortical networks in vivo. J. Neurosci. *29*, 9011–9025. https://doi.org/10.1523/JNEUROSCI.5646-08.2009.
72. Murata, Y., and Colonnese, M.T. (2016). An excitatory cortical feedback loop gates retinal wave transmission in rodent thalamus. Elife *5*, e18816. https://doi.org/10.7554/eLife.18816.
73. Ray, S., Crone, N.E., Niebur, E., Franaszczuk, P.J., and Hsiao, S.S. (2008). Neural correlates of high-gamma oscillations (60-200 Hz) in macaque local field potentials and their potential implications in electrocorticography. J. Neurosci. *28*, 11526–11536. https://doi.org/10.1523/JNEUROSCI.2848-08.2008.
74. Whittingstall, K., and Logothetis, N.K. (2009). Frequency-band coupling in surface EEG reflects spiking activity in monkey visual cortex. Neuron *64*, 281–289. https://doi.org/10.1016/j.neuron.2009.08.016.
75. Cheyne, D.O. (2013). MEG studies of sensorimotor rhythms: a review. Exp. Neurol. *245*, 27–39. https://doi.org/10.1016/j.expneurol.2012.08.030.
76. Hagiwara, K., Okamoto, T., Shigeto, H., Ogata, K., Somehara, Y., Matsushita, T., Kira, J.i., and Tobimatsu, S. (2010). Oscillatory gamma synchronization binds the primary and secondary somatosensory areas in humans. Neuroimage *51*, 412–420. https://doi.org/10.1016/j.neuroimage.2010.02.001.
77. Song, W., and Francis, J.T. (2015). Gating of tactile information through gamma band during passive arm movement in awake primates. Front. Neural Circuits *9*, 64. https://doi.org/10.3389/fncir.2015.00064.
78. Ray, S., and Maunsell, J.H.R. (2010). Differences in gamma frequencies across visual cortex restrict their possible use in computation. Neuron *67*, 885–896. https://doi.org/10.1016/j.neuron.2010.08.004.
79. Buzsáki, G., and Wang, X.J. (2012). Mechanisms of gamma oscillations. Annu. Rev. Neurosci. *35*, 203–225. https://doi.org/10.1146/annurev-neuro-062111-150444.
80. Cardin, J.A. (2016). Snapshots of the Brain in Action: Local Circuit Operations through the Lens of γ Oscillations. J. Neurosci. *36*, 10496–10504. https://doi.org/10.1523/JNEUROSCI.1021-16.2016.
81. Cardin, J.A. (2018). Inhibitory Interneurons Regulate Temporal Precision and Correlations in Cortical Circuits. Trends Neurosci. *41*, 689–700. https://doi.org/10.1016/j.tins.2018.07.015.
82. Roach, B.J., and Mathalon, D.H. (2008). Event-related EEG time-frequency analysis: an overview of measures and an analysis of early gamma band phase locking in schizophrenia. Schizophr. Bull. *34*, 907–926. https://doi.org/10.1093/schbul/sbn093.
83. Javitt, D.C., and Sweet, R.A. (2015). Auditory dysfunction in schizophrenia: integrating clinical and basic features. Nat. Rev. Neurosci. *16*, 535–550. https://doi.org/10.1038/nrn4002.
84. Roach, B.J., D'Souza, D.C., Ford, J.M., and Mathalon, D.H. (2019). Test-retest reliability of time-frequency measures of auditory steady-state responses in patients with schizophrenia and healthy controls. Neuroimage. Clin. *23*, 101878. https://doi.org/10.1016/j.nicl.2019.101878.
85. Welle, C.G., and Contreras, D. (2016). Sensory-driven and spontaneous gamma oscillations engage distinct cortical circuitry. J. Neurophysiol. *115*, 1821–1835. https://doi.org/10.1152/jn.00137.2015.
86. Adesnik, H. (2018). Layer-specific excitation/inhibition balances during neuronal synchronization in the visual cortex. J. Physiol. *596*, 1639–1657. https://doi.org/10.1113/JP274986.
87. Neuenschwander, S., Castelo-Branco, M., Baron, J., and Singer, W. (2002). Feed-forward synchronization: propagation of temporal patterns

along the retinothalamocortical pathway. Philos. Trans. R. Soc. Lond. B Biol. Sci. *357*, 1869–1876. https://doi.org/10.1098/rstb.2002.1172.

88. Saleem, A.B., Lien, A.D., Krumin, M., Haider, B., Rosón, M.R., Ayaz, A., Reinhold, K., Busse, L., Carandini, M., and Harris, K.D. (2017). Subcortical Source and Modulation of the Narrowband Gamma Oscillation in Mouse Visual Cortex. Neuron *93*, 315–322. https://doi.org/10.1016/j.neuron.2016.12.028.

89. Sirota, A., Montgomery, S., Fujisawa, S., Isomura, Y., Zugaro, M., and Buzsáki, G. (2008). Entrainment of neocortical neurons and gamma oscillations by the hippocampal theta rhythm. Neuron *60*, 683–697. https://doi.org/10.1016/j.neuron.2008.09.014.

90. Valiullina, F., Akhmetshina, D., Nasretdinov, A., Mukhtarov, M., Valeeva, G., Khazipov, R., and Rozov, A. (2016). Developmental Changes in Electrophysiological Properties and a Transition from Electrical to Chemical Coupling between Excitatory Layer 4 Neurons in the Rat Barrel Cortex. Front. Neural Circuits *10*, 1. https://doi.org/10.3389/fncir.2016.00001.

91. Daw, M.I., Ashby, M.C., and Isaac, J.T.R. (2007). Coordinated developmental recruitment of latent fast spiking interneurons in layer IV barrel cortex. Nat. Neurosci. *10*, 453–461. https://doi.org/10.1038/nn1866.

92. Kirmse, K., Kummer, M., Kovalchuk, Y., Witte, O.W., Garaschuk, O., and Holthoff, K. (2015). GABA depolarizes immature neurons and inhibits network activity in the neonatal neocortex in vivo. Nat. Commun. *6*, 7750. https://doi.org/10.1038/ncomms8750.

93. Dobbing, J., and Sands, J. (1979). Comparative aspects of the brain growth spurt. Early Hum. Dev. *3*, 79–83. https://doi.org/10.1016/0378-3782(79)90022-7.

94. Huttenlocher, P.R., and Dabholkar, A.S. (1997). Regional differences in synaptogenesis in human cerebral cortex. J. Comp. Neurol. *387*, 167–178. https://doi.org/10.1002/(sici)1096-9861(19971020)387:2<167::aid-cne1>3.0.co;2-z.

95. Khazipov, R., Esclapez, M., Caillard, O., Bernard, C., Khalilov, I., Tyzio, R., Hirsch, J., Dzhala, V., Berger, B., and Ben-Ari, Y. (2001). Early development of neuronal activity in the primate hippocampus in utero. J. Neurosci. *21*, 9770–9781. https://doi.org/10.1523/JNEUROSCI.21-24-09770.2001.

96. Xu, G., Broadbelt, K.G., Haynes, R.L., Folkerth, R.D., Borenstein, N.S., Belliveau, R.A., Trachtenberg, F.L., Volpe, J.J., and Kinney, H.C. (2011). Late development of the GABAergic system in the human cerebral cortex and white matter. J. Neuropathol. Exp. Neurol. *70*, 841–858. https://doi.org/10.1097/NEN.0b013e31822f471c.

97. Arshad, A., Vose, L.R., Vinukonda, G., Hu, F., Yoshikawa, K., Csiszar, A., Brumberg, J.C., and Ballabh, P. (2016). Extended Production of Cortical Interneurons into the Third Trimester of Human Gestation. Cereb. Cortex *26*, 2242–2256. https://doi.org/10.1093/cercor/bhv074.

98. Luhmann, H.J., Kirischuk, S., Sinning, A., and Kilb, W. (2014). Early GABAergic circuitry in the cerebral cortex. Curr. Opin. Neurobiol. *26*, 72–78. https://doi.org/10.1016/j.conb.2013.12.014.

99. Whitehead, K., Pressler, R., and Fabrizi, L. (2017). Characteristics and clinical significance of delta brushes in the EEG of premature infants. Clin. Neurophysiol. Pract. *2*, 12–18. https://doi.org/10.1016/j.cnp.2016.11.002.

100. Bourel-Ponchel, E., Gueden, S., Hasaerts, D., Héberlé, C., Malfilâtre, G., Mony, L., Vignolo-Diard, P., and Lamblin, M.D. (2021). Normal EEG during the neonatal period: maturational aspects from premature to full-term newborns. Neurophysiologie clinique = Clinical neurophysiology *51*, 61–88. https://doi.org/10.1016/j.neucli.2020.10.004.

101. Romagnoni, A., Colonnese, M.T., Touboul, J.D., and Gutkin, B.S. (2020). Progressive alignment of inhibitory and excitatory delay may drive a rapid developmental switch in cortical network dynamics. J. Neurophysiol. *123*, 1583–1599. https://doi.org/10.1152/jn.00402.2019.

102. Ray, S., and Maunsell, J.H.R. (2015). Do gamma oscillations play a role in cerebral cortex? Trends Cogn. Sci. *19*, 78–85. https://doi.org/10.1016/j.tics.2014.12.002.

103. de Villers-Sidani, E., Chang, E.F., Bao, S., and Merzenich, M.M. (2007). Critical period window for spectral tuning defined in the primary auditory cortex (A1) in the rat. J. Neurosci. *27*, 180–189. https://doi.org/10.1523/JNEUROSCI.3227-06.2007.

104. Woolf, N.K., and Ryan, A.F. (1988). Contributions of the middle ear to the development of function in the cochlea. Hear. Res. *35*, 131–142. https://doi.org/10.1016/0378-5955(88)90112-8.

105. Wess, J.M., Isaiah, A., Watkins, P.V., and Kanold, P.O. (2017). Subplate neurons are the first cortical neurons to respond to sensory stimuli. Proc. Natl. Acad. Sci. USA *114*, 12602–12607. https://doi.org/10.1073/pnas.1710793114.

106. Wang, H.C., Lin, C.C., Chong, R., Zhang-Hooks, Y., Agarwal, A., Ellis-Davies, G., Rock, J., and Bergles, D.E. (2015). Spontaneous Activity of Cochlear Hair Cells Triggered by Fluid Secretion Mechanism in Adjacent Support Cells. Cell *163*, 1348–1359. https://doi.org/10.1016/j.cell.2015.10.070.

107. Tritsch, N.X., Yi, E., Gale, J.E., Glowatzki, E., and Bergles, D.E. (2007). The origin of spontaneous activity in the developing auditory system. Nature *450*, 50–55. https://doi.org/10.1038/nature06233.

108. Khazipov, R., Sirota, A., Leinekugel, X., Holmes, G.L., Ben-Ari, Y., and Buzsáki, G. (2004). Early motor activity drives spindle bursts in the developing somatosensory cortex. Nature *432*, 758–761. https://doi.org/10.1038/nature03132.

109. Akhmetshina, D., Nasretdinov, A., Zakharov, A., Valeeva, G., and Khazipov, R. (2016). The Nature of the Sensory Input to the Neonatal Rat Barrel Cortex. J. Neurosci. *36*, 9922–9932. https://doi.org/10.1523/JNEUROSCI.1781-16.2016.

110. André, M., Lamblin, M.D., d'Allest, A.M., Curzi-Dascalova, L., Moussalli-Salefranque, F., S Nguyen The, T., Vecchierini-Blineau, M.F., Wallois, F., Walls-Esquivel, E., and Plouin, P. (2010). Electroencephalography in premature and full-term infants. Developmental features and glossary. Neurophysiologie clinique = Clinical neurophysiology *40*, 59–124. https://doi.org/10.1016/j.neucli.2010.02.002.

111. (GNU Octave software); J.W. Eaton, D. Bateman, S. Hauberg, R. Wehbring (2024). https://www.gnu.org/software/octave/doc/v9.3.0/.

112. Tadel, F., Baillet, S., Mosher, J.C., Pantazis, D., and Leahy, R.M. (2011). Brainstorm: a user-friendly application for MEG/EEG analysis. Comput. Intell. Neurosci. *2011*, 879716. https://doi.org/10.1155/2011/879716.

113. Qin, Y., Xu, P., and Yao, D. (2010). A comparative study of different references for EEG default mode network: the use of the infinity reference. Clin. Neurophysiol. *121*, 1981–1991. https://doi.org/10.1016/j.clinph.2010.03.056.

114. Acunzo, D.J., Mackenzie, G., and van Rossum, M.C.W. (2012). Systematic biases in early ERP and ERF components as a result of high-pass filtering. J. Neurosci. Methods *209*, 212–218. https://doi.org/10.1016/j.jneumeth.2012.06.011.

115. Tanner, D., Morgan-Short, K., and Luck, S.J. (2015). How inappropriate high-pass filters can produce artifactual effects and incorrect conclusions in ERP studies of language and cognition. Psychophysiology *52*, 997–1009. https://doi.org/10.1111/psyp.12437.

116. Maris, E., and Oostenveld, R. (2007). Nonparametric statistical testing of EEG- and MEG-data. J. Neurosci. Methods *164*, 177–190. https://doi.org/10.1016/j.jneumeth.2007.03.024.

117. The MathWorks Inc (2022). Statistics Toolbox Version: 9.1 (R2014b) (The MathWorks Inc). https://www.mathworks.com.

118. Gramfort, A., Luessi, M., Larson, E., Engemann, D.A., Strohmeier, D., Brodbeck, C., Parkkonen, L., and Hämäläinen, M.S. (2014). MNE software for processing MEG and EEG data. Neuroimage *86*, 446–460. https://doi.org/10.1016/j.neuroimage.2013.10.027.

119. Buitinck, L., Louppe, G., Blondel, M., Pedregosa, F., Mueller, A., Grisel, O., and Varoquaux, G. (2013). API design for machine learning software: experiences from the scikit-learn project. Preprint at: arXiv. https://doi.org/10.48550/arXiv.1309.0238

120. Maaten, L.V., and Hinton, G.E. (2008). Visualizing Data using t-SNE. J. Mach. Learn. Res. *9*, 2579–2605.

121. Noorlag, L., van Klink, N.E.C., Kobayashi, K., Gotman, J., Braun, K.P.J., and Zijlmans, M. (2022). High-frequency oscillations in scalp EEG: A systematic review of methodological choices and clinical findings. Clin. Neurophysiol. *137*, 46–58.

122. SAS Institute Inc (2020–2021). JMP® 16 Documentation Library (Chap. 16) (SAS Institute Inc. JMP®), pp. 1989–2023. Version 2020-2021.

123. Uusitalo, M.A., and Ilmoniemi, R.J. (1997). Signal-space projection method for separating MEG or EEG into components. Med. Biol. Eng. Comput. *35*, 135–140. https://doi.org/10.1007/BF02534144.

124. de Cheveigné, A. (2020). ZapLine: A simple and effective method to remove power line artifacts. Neuroimage *207*, 116356. https://doi.org/10.1016/j.neuroimage.2019.116356.

125. Delorme, A., and Makeig, S. (2004). EEGLAB: an open source toolbox for analysis of single-trial EEG dynamics including independent component analysis. J. Neurosci. Methods *134*, 9–21. https://doi.org/10.1016/j.jneumeth.2003.10.009.

STAR★METHODS

KEY RESOURCES TABLE

REAGENT or RESOURCE	SOURCE	IDENTIFIER
Deposited data		
EEG files including auditory stimuli, generated in this study (n=30)	Natus-Coherence EEG software Deltamed/Natus France.	https://doi.org/10.57745/XPXYHR (https://entrepot.recherche.data.gouv.fr/dataset.xhtml?persistentId=doi:10.57745/XPXYHR)
frequency power spectrum (PS) values of mean-referenced signals computed over 2-sec time intervals before and after the stimulus (using the Fast Fourier Transform) (raw values for each stimulus and mean values)	Natus-Coherence EEG software Deltamed/Natus France.	https://doi.org/10.57745/XPXYHR (https://entrepot.recherche.data.gouv.fr/dataset.xhtml?persistentId=doi:10.57745/XPXYHR)
Software and algorithms		
JMP Statistical Discovery software v.15-17	SAS Institute Inc.	
Natus-Coherence EEG software	Deltamed/Natus France.	https://natus.com
MATLAB R2014b	The MathWorks Inc.	https://www.mathworks.com
MATLAB Statistics Toolbox version: 9.1 (R2014b)	The MathWorks Inc.	https://www.mathworks.com
Brainstorm v. 3.230211 (11-Feb-2023)	University of Southern California	https://neuroimage.usc.edu/brainstorm
EEGlab	Matlab toolbox https://sccn.ucsd.edu/eeglab/ https://eeglab.org/tutorials/ConceptsGuide/statistics_theory.html	https://doi.org/10.1016/j.jneumeth.2003.10.009
Zapline	Matlab toolbox http://audition.ens.fr/adc/NoiseTools/src/NoiseTools/EXAMPLES/zapline/	https://doi.org/10.1016/j.neuroimage.2019.116356
Python MNE		https://doi.org/10.5281/zenodo.592483
Python Scikitlearn		https://jmlr.csail.mit.edu/papers/v12/pedregosa11a.html
GNU Octave -software	John W. Eaton, David Bateman, Søren Hauberg, Rik Wehbring (2019). numerical computations.	https://www.gnu.org/software/octave/doc/v9.3.0/
Codes depository	Mandeley data	https://doi.org/10.17632/7S382FS2BG.2
Other		
Clinical Research Study "Early EEG activities in preterm infant"	INSERM (French National Institute of Medical Research) Ethics Committee (N° 2751), N° ID-RCB: 2008-A0147-49	https://anr.fr/Projet-ANR-09-MNPS-0006

EXPERIMENTAL MODEL AND STUDY PARTICIPANT DETAILS

Subjects and EEG recording protocol

Participants and EEG recordings as well as the localization of electrode positions were described previously (figure S1).[8] These are summarized hereafter, along with description of additional stimuli and new analyses.

Subjects

Briefly, all premature newborns referred to the neonatal intensive care units (NICU) of Necker-Enfants Malades (Paris, France) or Bicêtre Hospitals (Kremlin–Bicêtre, France) from October 2013 to April 2014 and from November 2014 to December 2014, were

screened for inclusion. Only neonates without neurological risk were included in the study: inclusion criteria were as follows: age over 7 days, normal delivery, birth weight over the 10th percentile, spontaneous ventilation (nasal positive pressure was accepted), normal clinical examination, normal ultrasound scan performed by a pediatric radiologist (intra-ventricular hemorrhage grade I-II was accepted), normal otoacoustic emissions, no postnatal steroid treatment and no sedative drug within less than 4 days before the recording. EEG recordings were performed as part of routine neurological follow-up according to the recommendations for premature infants, at the patients' bedside.[110] Infants were prospectively followed by a trained neonatologist at 6 months, 1 year and 2 years of age, and were secondarily excluded from the analysis if psychomotor and neurological development was abnormal (1 case). Written informed consent was obtained from all parents. The procedure was in accordance with the Ethics Code of the World Medical Association, was approved by our institutional review board, INSERM (French National Institute of Medical Research) Ethics Committee (N° 2751), and was registered as a Clinical Research Study "Early EEG activities in preterm infant" (N° ID-RCB:2008-A0147-49), (French Research Agency https://anr.fr/Projet-ANR-09-MNPS-0006).

Thirty neonates were investigated, including 7 pairs of twins, 16 males, 14 females. Gestational age at birth (weeks of gestation) was 26-27 (n=1), 29-30 (n=2), 31-32 (n=11), 33-34 (n=14) and 35-36 (n=2) (Table S1). Age at recording was expressed as postmenstrual weeks (PMW = gestational age at birth + post-natal weeks). Clinical follow-up, was performed over 2 years, showing normal development at 2 years for 20 infants, and at one year for 3 infants; 7 infants were lost to follow-up.

EEG recording

Recordings were prospectively performed at the following PMW: 30-31 (n=2), 32-33 (n=8), 34-35 (n=8), 36-38 (n=12), according to the 10/10 international system and using 32 electrode neonatal caps (Wave Guard EEG neonatal cap, ANT-Neuro, certification CE, 3 sizes) (figure S1). They included cardiogram and respiration recording. Signals were sampled at 1024 Hz, amplified (1000 x), band-pass filtered at 0.16-334 Hz and digitized, using the Natus-Coherence EEG software (Deltamed/Natus, France).

Auditory stimuli

Auditory stimuli were diotically presented with constant sound volume via headphones. Stimulus consisted of a conventional 100-μs rectangular unfiltered alternating click at 70 dB sound pressure level (SPL) and a recorded male voice pronouncing the word "bébé" (meaning "baby" in French) recorded in the Waveform Audio File Format, lasting 420 ms, with a peak intensity of around 50 dB SPL, and a frequency peak at 400 Hz. Since good quality of EEG signal of AERs requires avoidance of movement artifacts and must be recorded when the infant is quiet, stimuli were presented during sleep and calibrated in order to prevent the child from waking. Stimuli were initiated as soon as the infant fell asleep, or when the infant was still sleeping despite the installation of the EEG caps. Stimuli were presented every 10 seconds (s). Stimulations began with the vocal stimulus, around 25 times, followed by presentations of the "click" stimulus until the baby woke up. The number of recorded auditory stimuli therefore depended on sleep duration. Recordings lasted no more than one hour. After offline screening of all responses and artifact rejection, the mean number of available stimuli for each baby was 30±21 (8-76) and 17±8 (7-43) for "click" and vocal stimulus respectively (Table S1).

Vigilance stage

Quiet sleep (QS) was defined by discontinuous, semi-discontinuous or "tracé alternant" EEG according to PMW, regular respiration and cardiac rhythms, with an absence of phasic movements disclosed by EEG artifacts and/or concomitant video recording. Active sleep (AS) was characterized by continuous activity, irregular respiration, and phasic movements.[51,100] The number of recorded auditory stimuli therefore depended on sleep duration. In 26 infants both stimuli were presented during the same vigilance stage (AS (24) and QS (2), while in 4 others auditory stimuli were presented in different vigilance stages (for details see Table S1).

METHOD DETAILS

Visual inspection of EEG

EEG preprocessing

EEG recording was first visually inspected (by AK) using the Natus-Coherence review program (Deltamed/Natus, France) to select artifact-free (electromyogram of facial and head muscles, movement, sweat, electrode dysfunction, eye movements, respiratory, interference from 220-volt 50-hertz alternating current (AC)) time intervals of 2 seconds (s) before and 2 s after stimuli. Recording on the Iz electrode was further removed as it was heavily artifacted leaving 31 electrodes for further analyses.

Detection of auditory-evoked responses

Auditory-evoked responses (AERs) including Delta-brushes (DBs) were visually identified on the raw EEG and marked at the time of the onset of the stimulus. Spontaneous DBs occurring at the main electrodes involved in AERs (FC6 and FC5 (pre-central inferior), T7 and T8 (mid-temporal) and CP6 and CP5 (temporal posterior) were also visually identified (A.K) across the entire EEG recording without artifacts and excluding the periods of 2 s before and after each stimulus and marked at the beginning of the negative deflection of the DBs.[8]

Neural oscillations in the gamma band

Oscillations in the gamma band (≥30 Hz) were visually searched on each individual raw EEG recording on the main electrodes involved in AERs (FC5, FC6, T7, T8, CP5, and CP6), after maximal amplification (1μV/mm) and on a one second full screen time scale

with application of 15.9Hz and 120Hz high and low pass filters respectively. Gamma oscillations were considered as true neural oscillations if there was a multicycle oscillatory pattern (at least 3 cycles) which clearly stood out from the background activity. Narrowband oscillations with discrete frequency peaks were identified using the power spectral density and wavelet analyze.

For the power spectrum density analysis of AERs (2 s before and after vocal and "click" stimuli) the raw data were exported from the Natus-Coherence software to an ascii file then imported and processed into GNU Octave.[111] An average montage was applied to the raw data which have been filtered by a 16Hz high pass filter and a 120Hz low pass filter. For each channels, 2 seconds data segments were extracted around each markers. The segments were detrended (mean of the segment removed), a Hanning window applied, the power spectrum of the segment calculated and finally the power spectrums averaged to generate the mean power spectrum. To facilitate the reading, a centroid was applied to the mean power spectrum (EEG review software Natus-Coherence; GNU Octave software).[65,111]

Delta-brush response rate

The DB response rate was calculated for each individual EEG recording, it was defined for both stimuli as the number of visually identifiable DBs evoked by the stimulus over the total number of the same type of stimuli. DBs were considered identifiable if response rate was >10% and easy identifiable if response rate was > 30%.[8] The response rates of evoked DBs after both stimuli were compared using a one-tailed paired Student's t-test.

Auditory event related potentials analyses (ERPs)

Auditory event-related potentials (ERPs) after both stimuli were obtained using individual and group level stimulus locked averaging of single AERs. Averaging was locked to stimulus onset for both stimuli. Comparative analyses at the individual and group level concerned the morphology of auditory ERPs: identification of peaks, their amplitude, latency and scalp topography.[35] ERPs after both stimuli were also assessed by principal component analysis (PCA) at group level. Brainstorm toolbox[112] along with home-made routines were used to determine ERPs by averaging AERs. Signals were down sampled to 256 Hz. The only digital filter applied to EEG data was the powerline filter (50 Hz and harmonics) by convolving the signal with a 20-ms boxcar window. To minimize signal distortion and as recommended for waveform analysis of ERPs, we used the minimal high pass filter of 0.16 Hz of our EEG device and an average reference, in order to avoid a systematic bias that could be induced by non-neutral referencing to the mastoid or vertex.[113–115] Signals were then screened visually and electrodes or segments showing artifacts were rejected from further analyses. Potentials were re-referenced to the average of all clean electrodes. Artifact-free epochs starting at -2 s and ending at +4 s relative to sound onsets were averaged separately for each individual subject and each stimulus type. The post-stimulus (0 to +4 s) potential at each time point was then compared against a baseline taken as the average potential over the 2 s preceding stimulus onset, separately for the two stimulus types, using statistical tests. A two-tailed, parametric Student's t-test was performed to compare the post-stimulus (0 to +4 s) potential at each time point against a baseline taken as the average potential over the 2 s preceding stimulus onset, separately for the two stimulus types. The threshold for significance was taken as $\alpha = 0.05$, corrected for multiple comparisons with the false discovery rate (FDR) method in the sensor and time domains.

Comparison of ERPs after both stimuli

For a fair comparison of auditory ERPs across stimulus types at the group level, an equal number of epochs were selected from each stimulus type, per subject, to re-compute individual averages. As all vocal stimuli were presented first, followed by "click" stimuli, epoch selection was performed as follows: if the number of available clean epochs for voice was larger than for "click" stimulus, the first vocal epochs were discarded; in the opposite case, the last "click" epochs were discarded. This rule ensured that all epochs were recorded at a similar time of the session and that the vigilance state of the subject was similar for both stimulus types. Balanced voice and "click" ERPs were compared at group level using a cluster-based permutation test over the 0-4 s post-stimulus period,[116] with $\alpha = 0.05$ as threshold for cluster significance. Cluster-based permutation tests solve the multi-comparison problem while accounting for the spatial and temporal correlations that exist among EEG time-series, so the significance threshold was not further corrected. To check whether any significant difference could be explained by an effect of the order of stimulus presentation, we performed a similar statistical comparison of the ERPs obtained after averaging of the first 5 versus the last 5 presentations, for each stimulus. Comparative analyses of peak latencies and amplitudes of voice and "click" evoked ERPs were performed in subjects who showed identifiable ERPs after both stimuli. ERP amplitudes and peak latencies were measured using the Natus-Coherence review program (Deltamed/Natus, France). To this end, ERPs were re-computed in Coherence using similar methods as in Brainstorm (see above). Latency was measured from the stimulus onset to the wave peak. Latency and amplitude were expressed as mean and standard deviation and compared across stimulus types using a one-tailed paired Student's t-test. We also measured the amplitude of N1 (200-400 ms) and N2 (400-1200 ms) ERP peaks in all infants (n=30) for both stimuli, computed the corresponding spatial maps and tested for significant differences between groups using a one-tailed paired Student's t-test.

Principal component analyses of ERPs

The principal component analysis (PCA) on both vocal and "click" ERPs was first performed after averaging of all available vocal and "click" stimuli from all infants. Preprocessing was performed with 30 Hz low pass filtering in addition to the 0.16Hz high pass filter of the EEG recording device. A mean reference excluding electrodes showing artifacts was used. PCA was computed on 31 channels in order to obtain PCs, their explained variance and the PCA scores as the projection of each channel in the principal component space.[117] To further compare PCs after both stimuli, we performed a PCA of epoch-averaged AERs to voice and "click" on the target electrodes showing the main ERPs after both stimuli. Three right and left mid-temporal, temporal posterior and pre-central inferior

(T7-8, CP5-6, and FC5-6) were used for the PC decomposition, but all electrodes were used for the visualization and analysis of component's topography. Processing was done with python using the MNE[118] and scikit-learn packages.[119] To assess the discriminative power of principal components, we used t-stochastic neighborhood embedding[120] over the principal component activations for each channel using the first two components (PC1 and PC2).

Frequency power spectrum (PS) analyses

PS variations after both stimuli

The frequency power spectrum (PS) of mean-referenced signals were computed over 2-sec time intervals using the Fast Fourier Transform (FFT) algorithm. The Log-transform of PS (Log PS) immediately preceding and following auditory stimuli were compared in 6 frequency bands usually used in EEG analyses, already used in preterm infants in clinical practice, and in event-related spectral perturbations (ERSPs) analyses in infants: delta=0.5-3.5Hz; theta=4-7.5Hz; alpha=8-13Hz; beta=13.5-29.5 Hz; gamma= 30-80 Hz and high-gamma > 80 Hz (limited to 198 Hz in our study).[79–81,121] To avoid artifacts from the powerline noise (50+/-0.5 Hz) and its harmonics (including their 1% of fluctuations) we removed 4 Hz from the FFT exports centered on 50, 100, 150 and 200 Hz. Gamma frequencies were therefore divided into gamma (30-48Hz and 52-80 Hz) and high-gamma (80.5-98 Hz;102-148 Hz and 152-198 Hz).[59,79,80,100,121]

Population statistical analysis of responses was performed separately for voice and "click", using a one-tailed paired Student's t-test for the difference between pre-and post-stimulus Log PS, considering the averaged Log PS for each individual. Additionally, the group Log PS increase (Log transform of power spectrum increase (Δ Log PS= Log PS' 2sec after stim') - (Log PS' 2sec before stim') after voice and "click" was compared by Welch's t-test assuming unequal variances. In the same way, the frequency power was compared in 5 frequency bands (delta to gamma) before and after the beginning of spontaneous DBs detected on electrodes of interest involved in AERs (FC5, FC6, T7, T8, CP5 and CP6).[8] All statistical comparisons on Log PS were performed for each electrode and for each frequency band separately. For the comparison of AERs after voice and "click", all stimuli were also included, without averaging of ΔLog PS. Left and right homologous electrodes were compared for their relative effects (where at least one was found significant) using one tailed paired t-tests.

The spontaneous DBs were similarly analyzed. The default threshold for statistical significance was set to $p < 0.05$. However, in those analyses where the responses were not averaged prior to the test, we applied the adjustment of significance level to $p < 0.01$ to fairly limit the occurrence of responses which increases with the gain in statistical power due to repetition of auditory stimuli.

To assess topographic correlations between PS variations after voice and "click" as well as after spontaneous temporal DBs, ΔLog PS was analyzed by frequency band, on each electrode in all infants, using a multivariate method of variable clustering based on the correlations between the 31 electrodes and using the Cluster Variables algorithm developed by SAS Institute Inc.[117] This approach is similar to a PCA as each variable cluster is represented by its first principal component (PC1), i.e., the linear component explaining the majority of the variance in this cluster's data. We identified the cluster members to identify groups of electrodes with similar variations, i.e. well represented by PC1. The number of clusters remained open, up to the limit to fulfill inclusion of all electrodes, a number varying with the spectral band and the stimulus type. Finally, the clusters were color-coded and 2D-mapped with respect to the relative position of the member electrodes, for visualization.

Simple and multiple linear regression analysis

After averaging individual responses (ΔLog PS) over epochs (post versus pre-stimulus), additional group-level statistical analyses of PS variations were performed using simple (F-test) and multiple linear regression model (least squares fitting) by including all electrodes, hemispheric location, gestational age (as a continuous variable in PMW), separately by frequency band and stimulus type. The effect of gestational age (as a continuous variable in PMW) on lateralization was assessed by a slope F-test after simple linear regression of the difference between responses (ΔLog PS) of each homologous electrode pair versus age. Data were further analyzed for interaction, using a model including the cross effects between electrodes as a factor and other variables of interest as above. These statistical procedures were performed using the JMP v.15-17 software.[122]

Time–frequency analyses

In delta to gamma frequency bands

The time-frequency (T-F) maps after vocal and "click" stimuli were made using Brainstorm.[103] To this end, T-F maps between -2 and +6 s relative to stimulus onset and between 1 and 45 Hz (1-Hz spacing) were re-computed with the latter toolbox, using a complex Morlet wavelet transform and the toolbox's default Gaussian kernel. The wavelet transform was applied after pre-processing as described in paragraph auditory event related potentials analyses. As heartbeats produced visible artifacts on time-frequency maps, preprocessed signals were further cleared of cardiac artifacts before time-frequency analysis. Heartbeats were detected and aligned using the electrocardiogram channel and the main cardiac artifact component was projected out of the EEG signals using Signal Space Projection.[123] Segments of 500 ms at the start and end of the resulting time-frequency maps were cut out to discard edge effects. Time-frequency magnitude maps were averaged across epochs for each individual subject and separately for voice and "click" conditions, using an equal number of epochs for both using the same selection method as for ERPs, (see methods section: comparison of ERPs after both stimuli). Event-Related Spectral Perturbations (ERSPs) were computed for each point of these average maps as the magnitude change, expressed as a percentage of the

average magnitude in a baseline taken between -1500 ms and -500 ms before stimulus onset. Further, ERSPs from voice and "click" conditions were directly compared using a two-tailed paired Student's t-test.

In alpha to high-gamma frequency bands

After removing the 50 Hz power line noise, commonly originating from electrical interference in the environment, using the Zapline tool,[124] time–frequency (T-F) analyses in the two EEG datasets from voice and "click" were computed with the EEGLAB toolbox[125] on the 6 target electrodes showing the strongest responses as disclosed by PS and ERPs, analyses using all available artifact free epochs. We preserved the sampling frequency of EEG acquisition, i.e., 1024 Hz. We used the markers "click" and voice to extract EEG epochs (from -2 to 2 s before and after the stimuli). The baseline-normalized spectrogram of the ERSPs was computed through a sinusoidal wavelet transform (Discrete Short Time Fourier Transform).[115] To determine the characteristics of the wavelet offering the best compromise between frequency and time resolution for studying the frequencies between 10 and 120 Hz, we varied the minimum number of cycles of the lowest frequency (from 2 to 11) and those of the highest frequencies (reaching from 10 to 90% of the number of cycles in the equivalent FFT window) of the Hanning-tapered window and we chose the best compromise visually. The baseline-normalized spectrogram of AERs was computed with wavelet cycles increasing linearly from 7 (at 10 Hz) to 50 (at 120 Hz). The time period between -1500 ms and -500 ms before stimulus onset was used as the baseline with a single-trial-based AERs baseline correction methods to reduce sensitivity to noisy trials. Finally, we masked the time-frequency figures to only display points with significance threshold set at $\alpha = 0.05$ using the statistical method of basic permutation after correcting for multiple comparisons (FDR method). To study the reproducibility of the event-related power between 3 and 40 Hz, with respect to stimulus onset, we studied the degree of phase-synchronization at each time-frequency point using the inter-trial phase coherence (ITC). As with any coherence measure, this feature, at a given time-frequency point, ranges from 0 (perfect phase asynchrony of oscillations within the different trials) to 1 (perfect phase synchrony).

Across the age groups

Maturational changes of neural oscillations in the delta to high gamma frequency band (3-120 Hz) were also assessed on target electrodes (FC5, FC6, T7, T8, CP5, and CP6) according to 3 age-groups: 30-32 PMW+6 days (group 1, n=5), 33-34 PMW+6 days (group 2, n=7) and 35-38 PMW + 6 days (group 3, n=18).

QUANTIFICATION AND STATISTICAL ANALYSES

The response rates of evoked DBs after both stimuli were compared using one-tailed paired Student's t-test (Table S1).

Significant deviations of ERP from pre-stimulus baseline (Figure 3A) were assessed by means of a parametric Student's t-test performed in Brainstorm, with threshold for significance set to $\alpha = 0.05$ and corrected for multiple comparisons with the false discovery rate (FDR) method in both the sensor and time domains.

Comparisons of ERPs between stimuli (Figures 3C and S2) were performed using a cluster-based permutation test in Brainstorm, with $\alpha = 0.05$ as threshold for cluster significance. Cluster-based permutation tests solve the multi-comparison problem while accounting for the spatial and temporal correlations that exist among EEG time-series, so the significance threshold was not further corrected.

For the individual and group-level averaging of auditory event related responses (AERs) and of event related potentials (ERP) amplitudes and peak latencies measures we used the Natus-Coherence review program (Deltamed/Natus, France). Latency and amplitude were expressed as mean and standard deviation and compared across stimulus types using a one-tailed paired Student's t-test. ERPs peaks amplitudes and latencies were tested for significant differences between groups using a one-tailed paired Student's t-test (Figure 4).

For the analyses of the frequency power spectrum (PS) variations after the auditory stimuli, mean-referenced signals were computed using the Fast Fourier Transform (FFT) algorithm and frequency PS values of 2-sec time intervals before and after the stimuli were exported using the Natus-Coherence EEG review software (Deltamed/Natus, France.

For comparisons before-after stimuli of Log-transform of power spectrum (Log PS) and of event-related potential (ERP) latency and amplitude, we used one-tailed paired Student's t test for analysis (Figures 6A and 6B; Tables S2 and S3).

For comparisons between independent voice and "click" stimuli responses (ΔLog PS), we used 2-tailed Welch's t test assuming unequal variances for analysis (Figure 6C).

For the determination of topographic correlations between PS variations (ΔLog PS) after auditive stimuli as well as after spontaneous temporal DBs, we used the multivariate clustering method with the "Cluster Variables" algorithm developed by SAS Institute Inc[117] for analysis (Figure S4).

For PS variations (ΔLog PS) after auditive stimuli left and right homologous electrodes were compared for their relative effects using one tailed paired t-tests (Table S5).

For evaluation of leverage effect of gestational age on lateralization of responses (ΔLog PS) we used a slope F-test after linear regression for analysis (Table S5).

For multiple linear regression analysis of responses, we used an ANOVA model of least squares fitting, and the cross effects between electrodes as a factor and other variables were also included into the model for analysis of interactions (Figure S5 and Table S6).

Differences were considered significant basically at $p < 0.05$, or at $p < 0.01$ in case of adjustment. JMP Statistical Discovery software v.15-17 was used for these statistical analyses (SAS Institute Inc.).

Computation of the PCA, t-stochastic neighborhood embedding and group analysis of PC1 and PC2 of the electrodes of interest-were done using Python MNE and scikit-learn packages. All statistical details for group comparison of component activation can be found in figure legend (Figure 5).

For computation and visualization of PCA on all electrodes for Figure S3 a MATLAB script was written using MATLAB PCA from the Statistics Toolbox version: 9.1 (R2014b), (Natick, Massachusetts: The MathWorks Inc.).

The comparison between stimuli of ERSP T-F maps spanning delta-to-gamma frequency bands (Figure 7) was performed using a two-tailed paired Student's test with significance threshold set at $\alpha = 0.05$ and corrected for multiple comparisons with the FDR method in the sensor, time and frequency domains.

For the statistical analyses of Time–frequency analyses from alpha to high-gamma frequencies, we masked the time-frequency figures to only display points with significance threshold set at $\alpha = 0.05$ using the statistical method of basic permutation after correcting for multiple comparisons (FDR method) provided by EEGLAB toolbox (for more details about statistical tests see https://eeglab.org/tutorials/ConceptsGuide/statistics_theory.html) (Figures 8, S6, and S7).

For the power spectrum density analysis of AERs (2 s before and after vocal and ''click'' stimuli) the raw data were exported from the Natus-Coherence software to an ascii file then imported and processed into GNU Octave[111] (Figure 9C).